



# New scaling paradigm for dynamics in glass-forming systems

Aleksandra Drozd-Rzoska, Sylwester J. Rzoska<sup>\*</sup>, Szymon Starzonek<sup>1,\*</sup>

*Institute of High Pressure Physics, Polish Academy of Sciences, ul. Sokolowska 29/37, 01-142 Warsaw, Poland*

## ARTICLE INFO

### Keywords:

Previtreous dynamics  
Scaling  
Glass transition  
Relaxation time  
Viscosity  
High pressures  
Dynamic crossover  
Polyols

## ABSTRACT

The lack of ultimate scaling relations for previtreous changes of the primary relaxation time or viscosity in glass-forming systems constitutes the grand fundamental challenge, also hindering the development of relevant material engineering applications. The report links the problem to the location of the previtreous domain remote from a hypothetical divergence, hidden in the solid glass state. As the solution, the distortions-sensitive and linearized derivative-based analysis is proposed. It is implemented to scaling relations being checkpoints of basic glass transition models: free volume, entropic, critical-like, avoided criticality, kinetically constrained, or Ising model related. For discussed scaling relations, alternative formulations based on fragility, the semi-universal metric for previtreous dynamics, are presented. The alternative approach based on the activation energy index, showing its relative changes, is also presented. Derived relations are validated for the primary relaxation time experimental data in the homologous series of polyols, from glycerol to sorbitol. Only two scaling equations passed the exam: MYEGA, the recent 'activation and critical' (AC), and their pressure counterparts. The report shows that the coherent picture linking (i) the Super-Arrhenius for the temperature path, (ii) the Super-Barus behavior for the pressure path, and anomalous changes detected on compressing, namely (iii) inflection, and (iv) viscosity decrease or speeding for relaxation time, is possible.

The report also shows the limited reliability of the so-called Stickel analysis and its pressure counterpart used for detecting the dynamic crossover in the previtreous domain.

## 1. Introduction

Vitrification and glass transition are common in nature [1–6] and essential for a variety of applications: from food [7], pharmaceuticals [8], cosmetics [9], polymers [10], modern materials engineering [11,12], chemical processing [13], and cryogenic implementations [14]. It also constitutes a grand fundamental challenge for which the long-awaited cognitive breakthrough has been expected for decades [15–19]. Consequently, one may ask why it is not happening yet?

The answer may provide a comparison with the *Physics of Critical Phenomena*, in which the descriptions of pretransitional effects on approaching the singular temperature (spinodal/pseudospinodal  $T_S$ , or critical  $T_C$ ) were the essential inspiration [20–28]. Related models predicted functional forms of pretransitional effects and values of relevant parameters, such as critical exponents [20,23,28]. The dominant impact of collective pretransitional fluctuations was identified as universal patterns source. The pretransitional behavior is described by power terms, linked to universal critical exponents, and limited to a single term very close to  $T_C$  ( $T_C + 1K$ ) [20,21].

<sup>\*</sup> Corresponding authors.

*E-mail addresses:* [arzoska@unipress.waw.pl](mailto:arzoska@unipress.waw.pl) (A. Drozd-Rzoska), [sylwester.rzoska@gmail.com](mailto:sylwester.rzoska@gmail.com) (S.J. Rzoska), [starzoneks@unipress.waw.pl](mailto:starzoneks@unipress.waw.pl) (S. Starzonek).

<sup>1</sup> Current address: Laboratory of Physics, Faculty of Electrical Engineering, University of Ljubljana, Tržaška 25, 1000 Ljubljana, Slovenia.

Such a simple description may extend even to a few tens of Kelvins for the mean-field type behavior [23–26,28]. Worth recalling is the case of weakly discontinuous phase transitions, where the singularity is hidden below a discontinuous phase transition temperature ( $T_m$ ), but ‘strong’ pretransitional anomalies still exist [20,22–29]. One may evoke the pseudospinodal behavior in near-critical liquids or the isotropic – mesophase transitions in liquid crystalline (LC) [23–26] and plastic crystalline (PC) systems [27,28]. They are characterized by the discontinuity metric  $\Delta T^* = T_m - T_s$  ranging from  $\Delta T^* = 1 - 2K$  for the isotropic liquid – nematic transition [20,23–25] to even  $\Delta T^* = 30K$  for transitions to highly ordered mesophases such as smectic E (SmE) in LCs [26] or orientationally disordered crystals (ODIC in PCs) [27,28]. Notably, even the ‘very weak’ discontinuity  $\Delta T^* = 1 - 2K$  can yield significant uncertainty in describing pretransitional effects if the nonlinear fitting is involved [23,29].

The glass transition is associated with pretransitional/previtreous effects starting 100 K or more above the glass temperature  $T_g$ , and manifesting for such dynamic properties as viscosity  $\eta(T)$  or the primary ( $\alpha$ ), structural) relaxation time  $\tau(T)$ . Surprisingly, after almost a century of studies, the portrayal of this phenomenon remains puzzling [17–19]. The experimental evidence indicates that previtreous effects can be portrayed by a single 3-parameter function in the range  $T_g < T < T_g + 80K$ . Generally, it is expressed by the heuristical Super-Arrhenius (SA) relation [16–19]:

$$\tau(T) = \tau_\infty \exp\left(\frac{E_a(T)}{RT}\right), \quad \eta(T) = \eta_\infty \exp\left(\frac{E_a(T)}{RT}\right) \quad (1)$$

where  $T > T_g$ ;  $R$  stands denotes the gas constant. The basic Arrhenius dependence is retrieved if  $E_a(T) = E_a = \text{const}$ , in the given temperature domain.

Worth stressing is the equivalence of the primary relaxation time  $\tau(T)$ , and the viscosity  $\eta(T)$  previtreous evolutions:  $\eta(T, P)/\eta(T_{ref}, P_{ref}) = C[\tau(T, P)/\tau(T_{ref}, P_{ref})]$ , where  $T_{ref}, P_{ref}$  are for the reference temperature and pressure,  $C = K(T, P)/K(T_{ref}, P_{ref})$ , and  $K$  stands for the bulk modulus [30]. Worth noting is also another link between these magnitudes:  $\tau(T, P) = (AV/k_B T)\eta(T, P)$ , where  $A$  is a system-dependent constant,  $V$  is molecular volume,  $T$  and  $P$  are for temperature and pressure, respectively [31]. This report is developed mainly in terms of  $\tau(T, P)$  to clarify the discussion.

The authors stress that previtreous ‘anomalies’ are associated with the ‘discontinuity’  $\Delta T_g^* = T_g - T_0 = 20 K - 50 K$ , or even more, where  $T_0 < T_g$  is the extrapolated singular temperature [16–19].

This report focuses on the comprehensive presentation of issues enabling the reduction of the parasitic impact of the huge discontinuity  $\Delta T_g^*$  on the reliable description of the previtreous effect, both for the temperature and pressure paths.

The SA concept is supported the normalized plot  $\log_{10}\tau(T)$  or  $\log_{10}\eta(T)$  vs  $T_g/T$  for the common presentation of dynamics in various glass-forming liquids, introduced by Angell et al. [32–35], for polymers and low molecular weight liquids. It was associated with the empirical ‘normalized’ assumption  $\tau(T_g) = 100s$  or  $\eta(T_g) = 10^{13}\text{Poise}$ . Angell et al. [32–35] also introduced the empirical metric for SA dynamics in various glass formers, namely the curvature at glass temperature called fragility ( $m$ ):

$$m = m_P(T \rightarrow T_g) = d\log_{10}\tau(T \rightarrow T_g)/d(T_g/T), \quad m = d\log_{10}\eta(T \rightarrow T_g)/d(T_g/T) \quad (2)$$

For the ‘Angell plot’ Arrhenius dynamics is a terminal reference, manifested by a straight line between ( $T_g/T = 1, \log_{10}\tau(T_g) = 2$ ) and ( $T_g/T = 0, \log_{10}\tau_\infty = -14$ ). Originally, the  $\tau_\infty = 10^{-14}s$  was assumed as an estimation of a typical value [25–29]. It yields  $m = \log_{10}\tau(T_g) - \log_{10}\tau_\infty = 16$  for the fragility for the basic Arrhenius behavior. Systems with a relatively weak deviation from such reference ( $m < 40-50$ ) are called ‘strong’ glass formers. Those related to  $m > 50$  are ‘fragile’ glass formers, with notable SA dynamics [32–35]. For the most fragile system, a limit value  $m = 220$  is indicated [36,37]. The fragility has become one of central concepts of the glass transition physics [16–19,31–38].

SA relation (Eq. (1)) enable a cognitive insight into the previtreous behavior, but not the parameterization of empirical data due to the unknown form of  $E_a(T)$  [24–27]. Consequently, replacement equations are required. The dominant position reached the Vogel-Fulcher-Tammann (VFT) relation [39–41], nowadays used in the form [17–19,42–44]:

$$\tau(T) = \tau_\infty \exp\left(\frac{\Phi}{T - T_0}\right) = \tau_\infty \exp\left(\frac{D_T T_0}{T - T_0}\right) \quad (3)$$

where  $T > T_g$ , extrapolated VFT singular temperature  $T_0 < T_g$  is usually located 20 – 100K below  $T_g$ ; the amplitude  $\Phi = D_T T_0 = \text{const}$ ,  $D_T$  is the fragility strength coefficient describing the degree of deviation from the basic Arrhenius pattern.

The comparison of Eqs. (1) and (3) yield the VFT formula for the apparent activation energy  $E_a(T)$ :

$$E_a(T) = (RD_T T_0)[(T - T_0)/T]^{-1} = (RD_T T_0)t^{-1} = Et^{-1}. E = \text{const} \quad (4)$$

The hypothetical universality of the VFT relation supported its applications for determining glass transition characterizations, basing on the analysis remote from  $T_g$ , for instance [34,38]:

$$m = \frac{D_T T_0 T_g}{(\Delta T_g^*)^2 \ln 10} \quad \text{or} \quad m = \mu \left(1 + \frac{\ln 10}{D_T}\right) \Rightarrow D_T = \frac{\mu \ln 10}{m - \mu} \quad (5)$$

where  $\Delta T_g^* = T_g - T_0$ ,  $\mu = m_{\min} = \log_{10}\tau(T_g) - \log_{10}\tau_\infty$ .

For macromolecular systems Williams-Landell-Ferry (WLF, 1955) relation [45], the VFT parallel, is most often used, as more convenient for some experimental methods, for instance rheological measurements [19]. VFT equation is related to three adjustable parameters: pre-exponential factor  $\tau_\infty$ , extrapolated singular temperature  $T_0$  and fragility strength  $D_T$ . This number is recognized as the optimal for scaling relations describing the pre-vitreous dynamics [16–19,34,35].

The extensive experimental evidence supporting the meaning of the VFT/WLF relations made them an empirical symbol of the pre-vitreous dynamics' universality [16–19,33–38]. Consequently, the derivation of VFT relation became a checkpoint for theoretical models [16–19,42,43]. However, none of the glass transition models manage to derive specific values of parameters in this equation [16–19,42,43]. This trend also strongly supports numerous experimental results suggesting a coincidence between the temperature  $T_0$  determined from dynamic studies and the Kauzmann temperature  $T_K$  (ideal glass) determined from the configuration entropy analysis, i.e., the thermodynamic insight [16–19,42–44,46–48]. Notwithstanding, the state-of-the-art analysis for 52 glass-formers carried out by Tanaka [49] showed that  $0.8 < T_0/T_K < 2.2$ , so the correlation  $T_0 \approx T_K$  can be considered only selected systems. Further, precise tests of the fragility determined via Eq. (5) revealed notable discrepancies with the direct estimation of the fragility index based on the 'Angell plot' [48,50]. Decisive arguments questioning the universality and fundamental significance of the VFT equation delivered the analysis based on the activation energy index (see below) [51–56]. Being inspired by these results, McKenna conducted a subtle study of the pre-vitreous effect in polymers using the WLF relation and showed a systematic rise of deviations when cooling toward the glass temperature  $T_g$  [53]. These results questioned the fundamental significance of VFT and WLF relations [44,45]. After decades of research, the most crucial experimental fact in the physics of glass transition turned out to be unknown. It seemed that only new 3-parameter model equations could overcome this cognitive deadlock [52].

The principal method of verifying new scaling equations is a visual or quantitative (residual) comparison of fitting quality for different experimental data sets [16–19,42,43,57–64]. However, such a classic analysis did not lead to a decisive prevalence of one model equation over another. This confusion may explain the mentioned non-accessibility of a domain in the vicinity of the singular temperature  $T_0$  with the most characteristic changes of  $\tau(T)$  or  $\eta(T)$ . Another way to prove the adequacy of a given scaling relation is a plot linking several dozen sets of experimental data for different glass-forming systems and obtaining a single scaling curve within overlapping data sets [58–69]. Such plots often serve as the essential empirical validations of the theoretical model matched to the given scaling relation. However, such analysis is performed using a three-parameters determined individually via fitting subsequent sets of experimental data. Hence, such superposition is a kind of the 'tautological validation', which success is guaranteed in advance.

But even with such weakly conclusive results, one may find that some equations offer a subtly better fit than others. Unfortunately, for other glass-forming systems, the situation seems to be flipped.

Hence, a question arises if a universal scaling equation for the pre-vitreous dynamics exists?

This report presents the innovative methodology for analyzing pre-vitreous effects that may respond to the above challenges. It bases on the linearized differential analysis sensitive to subtle disturbances between a scaling relation and experimental data. Contrary to the common practice, experimental validation tests are focused on a portrayal within a homologous series of glass-formers, with a systematic change of molecular structure symmetry. Finally, the state-of-the-art analysis of the pressure path approaching the glass transition is presented. It offers new reliable dependences able to portray not only the SB slowing down but also occurring in some systems the inflection behavior and the anomalous speeding up on compressing. In summary, it is stressed that the ultimate selection of the optimal scaling equation for the pre-vitreous dynamics, essential for the validation of the ultimate glass transition model, requires the analysis considering both temperature and pressure paths. The report present new conclusions regarding the dynamical crossover phenomenon, showing a limited reliability of the popular 'Stickel' method and its pressure counterpart.

## 2. VFT relation and its links to basic glass transition models

In 1889 Arrhenius [70] proposed the empirical formula for the temperature dependence of chemical reaction rates  $k(T) = k_\infty \exp(E_a/RT)$ . This relation introduced the concept of a process activation energy, easily determined from the linearized plot  $\ln k(1/T) = \ln k_\infty + E_a(1/T)/R$ . It became the base for describing many thermally induced dynamic processes in physical chemistry, including viscosity (Guzman, 1913 [71], Raman 1923 [72] and Andrade, 1933 [73]), primary relaxation time (Williams, 1964 [74,75]) as well as diffusion or the electric conductivity changes. In the 20th century, the industrial revolution entered a stage where the detailed description of such behavior became important for technological implementations. However, it became clear that the behavior goes beyond the Arrhenius pattern for many systems. Vogel (1921, [39] for mineral oils (lubricants, fuels, petrochemical industry) as well as Tammann [40], and Fulcher [41], in response to the challenges of the glass industry, introduced an additional parameter to the Arrhenius relation creating the enhanced 'functional flexibility:  $\log_{10}\eta(T) = A + B/(T - T_0)$ . For example, with this relation's help, Fulcher successfully described changes in the viscosity of soda-lime glasses with various compositions ranging from 500 to even 1400 °C [41].

The universality of VFT and WLF relations in subsequent decadence caused its derivation to become the checkpoint for glass transition models [16–19,42,43]. Doolittle [76], Turnbull, and Cohen [77,78] considered the free volume concept allowing for a molecule, or a polymer segment [74] movement, reaching the output relation:

$$\tau = \tau_\infty \exp\left(\frac{\gamma v_{free}^*}{v_{free}}\right) = \tau_\infty \exp(\gamma\phi) \quad (6)$$

where  $v_{free}^*$  is a minimum required volume of void for the reorientation process,  $\gamma$  is an overlap factor that should lie between 0.5 and 1, and  $v_{free}$  is specific free volume; fraction coefficient:  $\phi = v_{free}^*/v_{free}$ .

Eq. (6) converts into the VFT Eq. (3), assuming  $\phi = A(T - T_0)$

Adam and Gibbs [79] visualized a supercooled liquid as a progressively self-organized cooperatively rearranging region (CRR), which arrangement is inversely proportional to the configurational entropy  $S_C$ . Hence, the configurational entropy  $S_C(T)$  decreases on cooling, coupled with the increase of particle number in CRRs. The primary relaxation time is interpreted as the rate needed to rearrange the region, and its evolution is expressed by model output relation [36]:

$$\tau(T) = \tau_\infty \exp \frac{z^* \Delta\mu}{k_B T} = \tau_\infty \exp \frac{B}{TS_C(T)} \quad (7)$$

where  $\Delta\mu$  denotes transition state activation energy,  $z^*$  is the temperature-dependent number of cooperatively rearranging molecular entities determined by macroscopic configurational entropy  $S_C$ , in such a way that  $z^*/s_c^* = N_A/S_C(T)$ , in which  $s_c^*$  stands for the entropy of the smallest number of rearranging molecular entities and  $N_A$  is the Avogadro number.

Experimentally, configurational entropy  $S_C(T)$  is estimated from the evolution of the heat capacity excess  $\Delta C_p(T)$  [16–19,80]:

$$S_C = \int_{T_K}^T \frac{\Delta C_p(T)}{T} dT \quad (8)$$

In practice, it is assumed  $\Delta C_p(T) = C_p^{Liq} - C_p^{SolidGlass}$ , with the heat capacity of glass, instead of solid crystal entropy changes, hardly detectable in glass formers. VFT equation is retrieved if the following behavior for heat capacity and configurational entropy is assumed [18,19,42,80]:

$$S_C(T) = S_0 \left(1 - \frac{T_K}{T}\right) = S_0 \left(\frac{T - T_K}{T}\right) = S_0 t \quad (9)$$

where  $S_0$  describes high temperature entropy and  $T_K$  is the Kauzmann temperature.

Notably, Eq. (9) constitutes the essential tool for estimating the Kauzmann temperature [16–19,81] from the evolution of the configurational entropy. Its derivation is based on the ‘rough’ approximation of the specific heat capacity, which is in only qualitative agreement with experimental data. Hence, the crucial validation is related to obtaining the VFT Eq. (3) when Eq. (9) is substituted to Eq. (7).

The random first-order field theory (RFOT), also known as the mosaic theory, assumes the nucleation of ‘entropic droplets’ between different metastable configurations, creating a patchwork of local metastable configurations in a supercooled liquid [42,82,83]. It predicts the link between the primary ( $\alpha$ , structural) relaxation time, static length scale  $\xi(T)$  and configurational entropy  $S_C(T)$  [82–84]:

$$\tau(T) = \tau_\infty \exp \left( \frac{A \xi^\psi}{T} \right) \text{ and } \xi(T) \propto \left( \frac{1}{S_C(T)} \right)^{\frac{1}{d-\theta}} \quad (10)$$

where  $d$  is a spatial dimension,  $\theta$  is an exponent related to interface energy ( $Y$ ) changes between two amorphous states. The exponent  $\psi$  is related to a free energy barrier to overcome when rearranging a correlated volume of  $\xi$  size. Model-values linking exponent to a specific glass former have not been computed yet. Comparing Eqs. (7) and (10), the enhanced AG model equation emerges [84]:

$$\tau(T) = \tau_\infty \exp \left( \frac{A_G}{T(S_C)^\alpha} \right) \quad (11)$$

where the exponent  $\alpha = \psi/(d - \theta)$ .

This basic RFOT relation can be reduced to VFT dependence if the exponent  $\psi = d - \theta$  and  $TS_C(T) = (T - T_K)$ .

Tanaka [85] considered a pretransitional behavior as a critical-like and Ising-like phenomenon and derived the relation  $\tau(T) = \tau_\infty \exp D_T (\xi(T)/\xi_\infty)^{d/2}$ , where the correlation length  $\xi(T) = \xi_\infty (T - T_K)^{\nu=2/d}$  is associated with the singularity at the extrapolated Kauzmann temperature.

As described above, basic problems of VFT parameterization are inspired by the development of alternative scaling relations, particularly without the finite temperature divergence. The leading position seems to gain Mauro-Yue-Ellison-Gupta-Allan (MYEGA) dependence [86], for which configurational entropy is considered within the topological constraint model as  $S_C(T) = f_t(T) N k_B \ln \Omega$ , where  $N$  is the number of species (atoms, molecules),  $k_B$  is the Boltzmann factor, and  $\Omega$  is the number of degenerate configurations per floppy mode. Subsequently, the two-state model for topological degrees of freedom, for which network constraints are either intact or broken, was implemented. Relating the energy difference  $H(T)$  to enthalpy, it was derived that  $f_t(T) = 3 \exp(-H/k_B T)$ . The final substitution of the configurational entropy into AG model Eq. (11) led to MYEGA equation, with the name recalling the authors of ref. [86]:

$$\tau(T) = \tau_\infty \exp \left[ \frac{C}{T} \exp \left( \frac{K}{T} \right) \right] \quad (12)$$

where  $K = A_{AG}/3Nk_B \ln \Omega$  and  $C = H/K$  are constants.

It can be approximated by VFT dependence assuming the validity of first-order term Taylor series expansion [59]:

$$\ln\left(\frac{\tau(T)}{\tau_\infty}\right) = \frac{C}{T} \exp\left(\frac{K}{T}\right) = \frac{C}{T \exp(-K/T)} \approx \frac{C}{T(1-K/T)} = \frac{C}{T-K} \quad (13)$$

This yields the VFT equation for  $K = T_0$  and  $C = D_T T_0$ .

Models described above consider the VFT, or alternatively WLF, relation as a peculiar universal pattern of pre-vitrification dynamics. The appearance of this relationship in the qualities of various glass systems made it possible to explain the extraordinary pre-vitrification effects, such as the consequences of free volume or configuration entropy on a global (macro) scale, as in the AG [79] or MYEGA [86] models, or local (micro), related to the appearance of heterogeneity with an increasing radius correlation (RFOT) [82–84].

There are also models suggesting the need for some significant modifications in the reference VFT relation. The free volume Cohen-Grest (CG) model is perhaps the most common reference [87]. It treats the supercooled dynamics considering diffusion in a system divided in liquidlike and solid-like cells, only the former having free volume. The model resulted in SA-type checkpoint relation most often presented in the following form [87]:

$$\log_{10}\tau(T) = A_{CG} + \frac{B_{CG}}{T - T_0 + [(T - T_0)^2 + C_{CG}]^{1/2}} \quad (14)$$

where  $A_{CG}$ ,  $B_{CG}$ ,  $C_{CG}$ , and singular temperature  $T_0$  is linked to the percolation threshold reached when each liquidlike molecule is proximate to at least two other liquid-like molecules.

Notably, CG Eq. (4) contains 4 adjustable parameters, i.e., more than VFT-related equation discussed above.

Rössler et al. [88] proposed yet another SA-type broad temperature range previtreous portrayal, assuming that the activation energy is the sum of two contributions:  $E_a(T) = E_\infty + E_{coop}(T)$ , where  $E_a = const$  is the high-temperature activation energy and  $E_{coop}(T)$  is the activation energy for the cooperative energy, varying exponentially with  $T$ . These yielded the SA-type relation, most often presented in the following form [88]:

$$\log_{10}\tau(T)/\tau_\infty = \frac{E_\infty + a \exp(-\lambda(T/T_A - 1))}{T} \quad (15)$$

where  $T_A$  is the crossover temperature from the Super-Arrhenius to Arrhenius behavior in high-temperature regions, described solely by  $E_\infty$  activation energy.

In the title, ref. [88] the above relationship is referred to as 3-parameter scaling relation, although it contains as many as 5 parameters:  $\tau_\infty$ ,  $\lambda$ ,  $a$ ,  $T_A$ ,  $E_\infty$ . It results from the apriori assumption that the precise estimation of  $E_\infty$ ,  $T_A$  and even the prefactor  $\tau_\infty$  is always possible, thus yielding extremely reliable fitting. This is validated for 15 glass-forming liquids, including glycerol, discussed as an example material in the given. Unfortunately, the existing experimental evidence and the practice of the authors of this work show that the explicit transition to the Arrhenius domain is rarely achieved. Moreover, in the dynamic low-temperature domain, most often in the  $T_g < T < T_g + 80K$  range, it is inherently impossible to reach the Arrhenius domain. Hence, it is difficult to recognize the above relations as 2 or 3 parameters scaling equations.

CG model Eq. (14) [87] is related to 4, Roessler et al. Eq. (15) [88] even 5 adjustable parameters. It ‘guarantees’ the high reproducibility of  $\tau(T)$  experimental data in the previtreous domain, but at the cost of a very large absolute error in parameters fitted. For such reasons, this report will not discuss multi-parameter (4, 5, ...) relations, recalling the VFT equation as the reference. This reports report focuses on 3-parameters relations for describing the previtreous dynamics, indicated as the most optimal, regarding the relationship between the reproducibility of experimental data and the real experimental error of parameters.

When discussing VFT-type relations, notable are also ‘extended’ relations that introduce the additional power exponent [89–91]:

$$\tau(T) = \tau_\infty \exp\left(\frac{\Phi}{(T - T_0)^\theta}\right) \quad (16)$$

Formally, the exponent increases the number of parameters to 4, but there are models defining its value. Bendler et al. [89,90] linked the ultraviscous/ultraslow behavior to the appearance of local and temporary mobile defects. In the Defect Diffusion Model (DDM) model, supercooled liquid is considered a binary solution of defected and non-defected structures. ‘Phase separation’ should have occurred at the crystallization temperature, with the formation of a translationally and rotationally ordered crystal phase and simultaneous disappearance and conversion of defect to ordered structures. In complex glass-forming materials, a large nucleation barrier to crystallization permits supercooling of the disordered ‘mixture,’ trapping ‘dissolved’ defects and preventing their reorganization and conversion to the lower free-energy structural units. If the free-energy mismatch and defect density are high enough, pretransitional fluctuations and correlations become evident before  $T_g$  is reached, leading to Eq. (16) with exponent  $\theta = 3/2$ . In DDM model, the singular temperature  $T_0$  is interpreted as the temperature at which a binary consolute point would occur if the system mobility (on the time scale of the experiment) did not vanish first. The generic link of the DDM to the percolation phenomenon causes is often considered for describing DC electric conductivity  $\sigma$  in glassy ionic liquids. In such a case, one should consider the impact of the translational-orientational ( $t$ - $o$ ) decoupling in the low-temperature dynamic domain. Its generalized form, taking into account both temperature ( $T$ ) and pressure ( $P$ ) paths:  $[\tau(T, P)]^s \sigma(T, P) = cT \Rightarrow \sigma^{-1} = \sigma_\infty^{-1} \tau^s$ , where  $c, \sigma_\infty = const$  and  $s \leq 1$  is the decoupling exponent: the  $t$ - $o$  coupling occurs for  $s = 1$ . The latter is expected in the high-temperature dynamic domain, although exceptions from this rule were also noted.

Very recently, Chamberlin [91] considered Ising Model with Orthogonal dynamics (OIM) for explaining the previtreous dynamics properties of supercooled glassy liquids. The model allows energy conservation and angular momentum to proceed independently on their preferred time scales. It also includes a unique step that makes or breaks the interaction between neighboring spins, facilitating an equilibrium distribution of bond energies. Within the mean-field approximation, it yields the following dependence [91]:

$$\tau(T) = \tau_{\infty} \exp\left[\frac{1/C}{(1 - T_c/T)^2}\right] = \tau_{\infty} \exp\left[\frac{T^2/C}{(T - T_c)^2}\right] \tag{17}$$

In the above relation, the original notation of ref.[17] is preserved, where  $T_c$  is explained as resembling the Curie-Weiss type ‘critical’ divergence temperature.

Eq. (14) with the exponent  $\theta = 2$ , called VFT2 in ref. [17]. I, that the possibility of emerging the additional term ‘VFT4’. The test of VFT2, is some cases supplemented by VFT4 relation, is the crucial validation for the OIM model. It has been carried out for 5 supercooled liquids, including glycerol, via the residual analysis, compared with VFT and MYEGA relations fitting. It is supplemented by Stickel-type derivative analysis [91,92], which is discussed in subsequent sections. One should note that linking VFT2 and VFT4 relations increases the number of parameters to 6.

The above resume shows the essential significance of VFT type portrayal of the previtreous effect for basic glass transition model. The problem emerges when taking into account references, recalled at the end of the Introduction section, questioning two paradigmatic assumptions: (i) the correlation between the ‘dynamic singularity’ ( $T_0$ ) associated with  $\tau(T)$  evolution, and the ‘thermodynamic singularity’ i.e., Kauzmann temperature ( $T_K$ ) related and configurational entropy changes [93], (ii) the omnipotence and fundamental validity of the VFT equation. The latter offers only an effective portrayal, limited to selected glass systems. Notwithstanding, usage of the VFT equation in experimental, theoretical, and practical applications has grown permanently in the last decades, as illustrated in Fig. 1.

When discussing experimental validation of VFT Eq. (3), it is worth also recalling the analysis proposed by Stickel, [92] used to detect the dynamic crossover temperature  $T_B$  [42,68,82,92,94,95]. It is realized by the transformation of experimental data  $\tau(T) \rightarrow \varphi_T = [d\log_{10}\tau(T)/d(1/T)]^{-1/2}$ , and plot  $\varphi_T(T)$  vs  $1/T$ , yielding two lines intersecting at dynamic crossover temperature  $T_B$ . The latter separates ergodic (HT, high-temperature) and non-ergodic (LT, low-temperature) dynamic domains in the ultraviscous region [42,68,82,94,95]. In both domains, another optimal evolution of dynamic properties is predicted. For the HT one, for  $T > T_B + (10K\text{Å} \cdot 20K)$ , the description is very similar to an extrapolated singular temperature  $T_c^{MCT} \approx T_B$  [42,94,98,99]:

$$\tau(T) = \tau_0 (T - T_c^{MCT})^\gamma \tag{18}$$

where the exponent  $\gamma = 1.3 - 4$  is related to parameters describing the high-frequency part of the imaginary part of the dielectric permittivity spectrum [17,42].

The description in HT domain using relation (15) is well-founded within the mode-coupling theory (MCT). Usually  $T_B \approx 1.3T_g$ , which estimates the range of LT domain to  $80K\text{Å} \cdot 100K$  [17,42,94,98-100]. Novikov and Sokolov [68] strengthened the possible fundamental significance of  $T_B$  and  $\varphi_T(T)$  plot, by announcing the semi-universal ‘magic’ time scale  $\tau(T_{B\pm}) = 10^{-7\pm 1}s$ . This empirical finding was obtained by the use of  $\varphi_T(T)$  plots for 29 glass-forming low-molecular-weight liquids, polymers, ionic systems, covalent systems, and plastic crystals [84]. Notwithstanding, a few striking discrepancies from the ‘magic’ time-scale has been noted later [31,59,86,87]. Casalini and Roland [95] developed the above concept for pressure path on approaching glass transition via plot

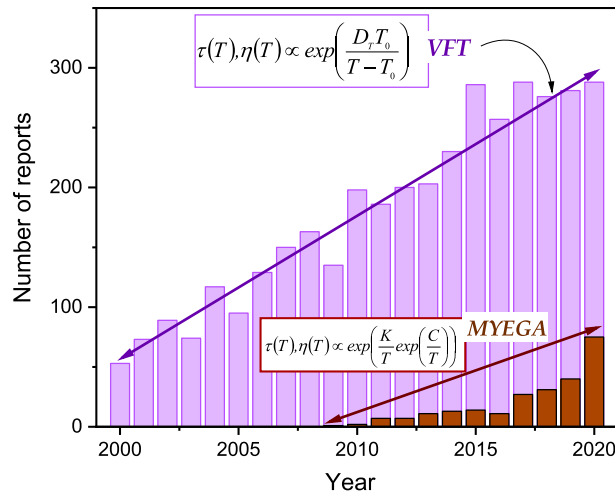


Fig. 1. Number of reports presenting VFT relation in the last two decades. It also shows many works using the MYEGA relation, which has been an essential alternative description of the pre-vitrification dynamics since 2010. Results were obtained using Google Scholar.

$(d\log_{10}\tau(P)/dP)^{-1/2}$  vs  $P$  and indicated empirical invariance  $\tau(T_{B\pm}, P_B) = 10^{-7\pm 1} s$  in the pressure–temperature plane. However, the question arises as to whether the Stickel analysis [92], closely related to VFT relation, is influenced by fundamental doubts about the latter? Another issue is that Stickel et al. [92] analysis assumed the preference for VFT description in both dynamic domains, while the experimental evidence indicates a universal tendency to prefer MCT Eq. (18) in HT dynamic domain.

### 3. Experimental

Studies were carried out in homologous series of polyols, from glycerol to sorbitol, for which changes in molecular structure lead to the emergence of the uniaxial molecular symmetry. They belong to classic glass-forming systems, which hardly crystallize when the melting temperature passes [34,42,101–107]. Such a feature facilitates broadband dielectric spectroscopy (BDS) studies, requiring frequency scans of the electric impedance, lasting several minutes or more for  $T \rightarrow T_g$  [103]. Compounds were purchased from Sigma-Aldrich, anhydrous, analytic quality grade, and used without additional purification. The measurement capacitor was filled in a dry box. The gap of the capacitor  $d = 0.2 mm$  and the voltage of the applied electric field  $U = 1 V$  were performed. The Quattro automatized unit supplemented the Novocontrol impedance analyzer for temperature control was used. These enabled the five-digit permanent resolutions for parameters, and the temperature stability was better than 0.1 K.

The research was focused on the primary (*alpha, structural*) relaxation time, determined using derivative analysis of the primary loss curve to find the location where  $d\log_{10}e''(f = f_{peak})/d\log_{10}f = 0$  what yields relaxation time  $\tau = 1/2\pi f_{peak}$ . Such an approach minimizes the fitting uncertainty, which may be significant for the most popular way of multi-parameter fitting of  $e''(f)$  loss curve using the Havriliak-Negami or related functions [105]. Obtained evolutions of primary relaxation time in tested compounds are shown in Fig. 2, using normalized Angell plot presentation. For such a plot, the Arrhenius behavior is referred to as linear. Increasing curvature illustrates the rising degree of SA behavior, characterized by fragility index  $m$ . It changes from  $m \approx 52$  for glycerol to  $m \approx 158$  for sorbitol, in agreement with earlier estimations [17,103]. This rise correlates with the emergence of uniaxial structures or the increasing importance of hydrogen bonding [17,102–107]. Generally, the previtreous dynamics of polyols are discussed concerning the essential role of hydrogen bonding. The emergence of local, preferably uniaxial structures increases the number of neighboring molecules, which yields more possibilities for hydrogen bonding and densifying –OH groups locally. A similar impact of the uniaxial form of molecules is well known in the isotropic liquid phase of rod-like liquid crystals. Consequently, there is no contradiction between the increasing role of hydrogen bonds and the less frequently discussed uniaxiality of molecular structure in discussed polyols. Instead, a synergy between mentioned factors may be expected.

### 4. Linearized, derivative-based analysis of the previtreous dynamics

Previtreous changes of dynamic properties, such as viscosity or primary relaxation time, start even more than 100 K above the glass temperature [103]. Their analysis via scaling relations is possible only remote from singular temperatures, such  $T_0$  in VFT Eq. (3). One may introduce the discontinuity metric  $\Delta T_g^* = T_g - T_0$ , which can even exceed 50 K [98,101,105]. It estimates the domain in the vicinity of singular temperature, which is non-accessible for analysis of  $\tau(T)$  or  $\eta(T)$  evolutions. Unfortunately, it is also a region with

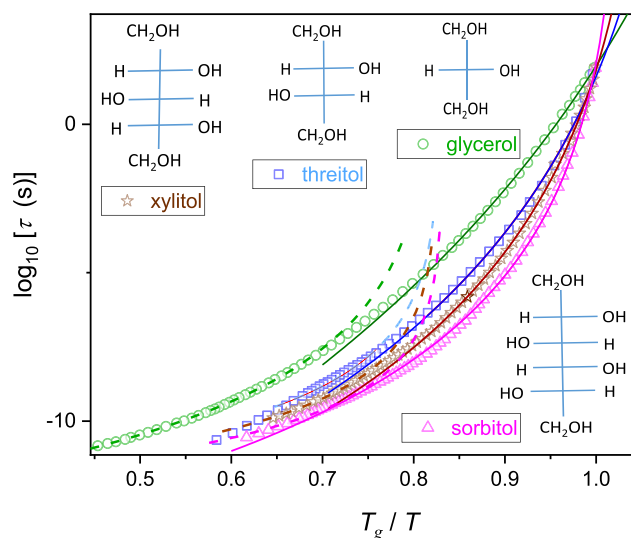


**Fig. 2.** Normalized Angell plot for previtreous changes of primary relaxation time in polyols: glycerol ( $T_g = 187.7$  K), threitol ( $T_g = 224.4$  K), xylitol ( $T_g = 247.6$  K), and sorbitol ( $T_g = 268.3$  K) [103–107]. Schematic structures of compounds are shown. Solid (low-temperature, non-ergodic dynamic domain) and dashed curves (high temperature, ergodic domain) are related to activation-critical relation Eq. (33), parameters are given in Table 1.

the most characteristic changes in these properties. The experimentally accessible region  $T > T_g = T_0 + \Delta T_g^*$  can be considered as the specific ‘long tail’ of previtreous changes. Consequently, the validation test of scaling relations based only on the visual or residual analysis cannot be decisive. The cognitive impasse can be overcome by using the linearized distortions-sensitive analysis discussed in this section. It bases on the distortions-sensitive transformation of experimental data, yielding linear behavior in the domain where the given scaling relation may be applied. The significant problem of scaling relations derived from glass transition models is that the latter does not yield specific values of parameters linked to the given experimental system [24–27,35–37,49,52,59,76,77,79]. To limit this problem, model scaling relations are also presented in terms of fragility, the surrogate empirical parameter characterizing the potential universality of dynamics in glass formers. Fragility constitutes a terminal of apparent fragility  $m_p(T \leq T_g)$ , also known as the steepness [42], which is directly linked to apparent activation enthalpy  $H_a(T)$ :

$$\tau(T) \rightarrow H_a'(T) = \frac{H_a(T)}{R} = \frac{d \ln \tau(T)}{d(1/T)} = \left( \frac{T_g}{\log_{10} e} \right) \frac{d \log_{10} \tau(T)}{d(T_g/T)} = (T_g \ln 10) m_p(T) \tag{19}$$

The discussion of basic model-relations starts from MYEGA Eq. (12), often indicated as a possible successor of VFT dependence grand success. It is finished with issues related to the basic SA-type VFT and critical-like (CL) portrayals and the recent relation linking these approaches. As described above, basic problems of VFT parameterization inspired the development of alternative scaling relations, particularly without finite temperature divergence. The leading position seems to gain Mauro-Yue-Ellison-Gupta-Allan (MYEGA) dependence [59]. Eq. (12) can also be expressed in fragility-related characteristics, namely  $K = \mu T_g = \text{const}$  and  $C = [(\mu - 1)T_g/T] - 1 = [(\mu - 1)T_g - T]/T$  [59].

Note that Eq. (12) may be alternatively derived from the basic free volume, assuming  $f = C' \exp(K/T)$ . Focusing on the linearized, distortions-sensitive test for MYEGA dependence [59], one obtains:

$$\frac{d \ln \tau(T)}{d(1/T)} = H_a'(T) = C \exp\left(\frac{K}{T}\right) + \frac{CK}{T} \exp\left(\frac{K}{T}\right) = \exp\left(\frac{K}{T}\right) \left[ C + \frac{CK}{T} \right] \rightarrow \ln H_a'(T) = \frac{K}{T} + \ln \left[ C \left( 1 + \frac{K}{T} \right) \right] \approx \frac{2K}{T} + \ln C = A \frac{1}{T} + B \tag{20}$$

Linear domain in the plot  $H_a'(T)/\exp(1/T)$  vs  $1/T$  indicates the region of applicability of MYEGA description. The linear regression yields parameters:  $K = B/A$ ,  $C = A/\exp K$ .

Fig. 3 shows tests for distortion-sensitive analysis via Eq. (20) of MYEGA Eq. (12). Linear domains appear for the low-temperature and high-temperature dynamical domains. It indicates MYEGA Eq. (12) possibilities to portray previtreous dynamics and a new way to test the dynamic crossover phenomenon.

Notwithstanding, determining the crossover temperatures  $T_B$  is associated with some arbitrariness, as visible in Fig. 3. However, it is even more pronounced for the commonly used ‘Stickel operator’ analysis [68,82,93–96], linked to the VFT relation (Eq. (3)), which fundamental significance can be questioned, as indicated in the given report.

Over three decades ago, Avramov and Milchev derived another scaling relation for the previtreous dynamics avoiding the finite temperature singularity [60]:

$$\tau(T) = \tau_\infty \exp\left(\frac{A_{AM}}{T^D}\right) \tag{21}$$

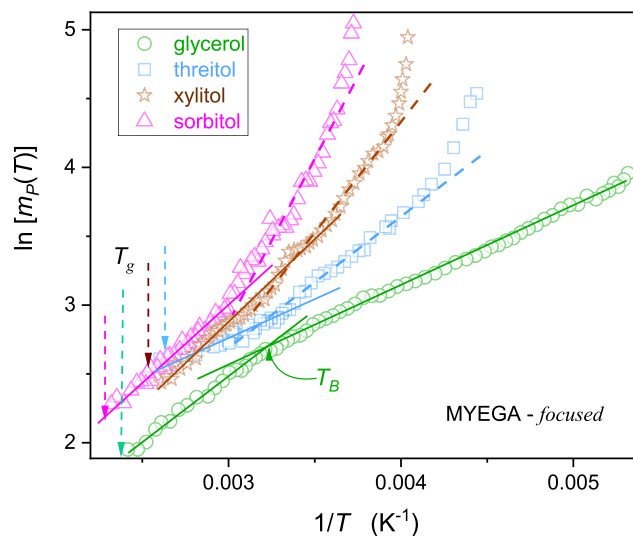


Fig. 3. Distortion-sensitive tests for preferable portrayal  $\tau(T)$  previtreous changes in polyols via MYEGA relation [59] (Eqs. (12)): such domains should follow linear patterns. Intersections of straight lines indicate possible dynamical crossover temperatures: (i) glycerol  $T_B = 312$  K, (ii) threitol  $T_B = 315$  K, (iii) xylitol  $T_B = 300$  K, and (iv) sorbitol  $T_B = 295$  K.

Applying the fragility concept, one may express this dependence in the ‘universal’ form  $D = m/\mu$ . Notably, link to the earlier Bässler equation for which  $D = 2$  [109]. Comparing AM Eq. (21) with Eqs. (6) and (7), one obtains  $f = C/T^D$  for free volume fraction and  $S_c \propto T^{D-1}$  for configurational entropy, disagreed with experimental evidence (see exp. results in [18,19,42]). Considering linearized, derivative-based test for AM Eq. (19), one obtains [110]:

$$\log_{10} \left[ \frac{d(\ln \tau)}{d(1/T)} \right] = \log_{10} H'_a = \log_{10}(CD) + (1-D)\log_{10} T = A + B \log_{10} T \tag{22}$$

For plot  $\log_{10} H'_a(T)$  vs  $\log_{10} T$ , linear behavior indicates the region of applicability of AM relation, and linear regression yields optimal values of parameters:  $D = 1 - B$  and  $C = 10^A/(1 - B)$ .

Fig. 4 presents the linearized, distortions-sensitive test of Avramov-Milchev [60] and Bässler [109] equations. The latter is considered one of the possible output relations for Kinetic Constraint Models (KCM) [94]. For the broader range of temperatures, the preference for AM Eq. (22) portrayal appears only for glycerol, but with the parameter  $D \neq 2$ .

In the last decade, notable efforts have been devoted to dynamic facilitation theories (DFT), particularly within KCM models frames [65,111–113]. They considered vitrification a purely kinetic phenomenon, for which movements of molecules in previtreous, supercooled regions are associated with excitations that appear/disappear in the adjacent areas. These facilitated dynamics develop in a hierarchical and correlated fashion in a specific direction. This picture emerges when cooling below inset temperature, associated with the Arrhenius–non-Arrhenius crossover. Chandler, Garrahan, and Elmatad (CGE) [65,111–113] derived the basic experimental checkpoint relation for KCM approaches, obeying the high-temperature Arrhenius – non-Arrhenius onset temperature  $T_o$  and the glass temperature  $T_g$  [65,111]:

$$\log_{10} \left( \frac{\tau(T)}{\tau_o} \right) = \left( \frac{J}{T_o} \right)^2 \left( \frac{T_o}{T} - 1 \right)^2 \Rightarrow \tau(T) = \tau_o \exp \left[ G \left( \frac{1}{T} - \frac{1}{T_o} \right)^2 \right] \tag{23}$$

where  $G = J^2/\ln 10$ .

For a large enough value of  $T_o$ , it may be approximated by the Bässler equation [108], which appears in the East model within the simplified DFT approach [111–113]. For the linear derivative-based test of CGE Eq. (21) the following relation can be derived:

$$m_p(T) = \frac{2J}{T_g} \left( \frac{1}{T} - \frac{1}{T_o} \right) = A \frac{1}{T} + B \tag{24}$$

For the plot  $m_p(T)$  or  $H'_a(T)$  vs  $1/T$  linear behavior validates the CGE Eq. (23) application for the glass former and in the given temperature domain. The subsequent linear regression yields optimal values of parameters  $J = A/2T_g$ ,  $T_o = A/B$ . One can also present Eq. (21) in terms of the ‘universal’ metric, fragility, substituting  $J^2 = (m/2) [T_g/(T_o/T_g - 1)]$ , as results from Eq. (24) for  $T = T_g$ . Eq. (23) is often recalled as the ‘parabolic relation’ for describing previtreous dynamics due to the Bässler-type approximation:  $\log_{10} \tau(T) \propto 1/T^2$  [110–112]. Overlapping of  $\tau(T)$  experimental data for 68 glass-forming systems in ref. [65], is recalled as a crucial argument supporting the universal meaning of CGE Eq.(21) and the experimental validation of DFT/KCM models. In the opinion of the authors, this experimental result (shown in ref. [65]) has tautological features and cannot be considered a conclusive validation of CGE Eq. (23), since the basic plot is scaled:  $\log_{10}(\tau/\tau_o)$  vs  $(J/T_o)^2(T_o/T - 1)^2$ , i.e., using all adjustable parameters included in Eq. (21), individually for each selected glass-formers. Similarly, 3-parameters-based scaling plots showing overlapping of experimental data are known for other

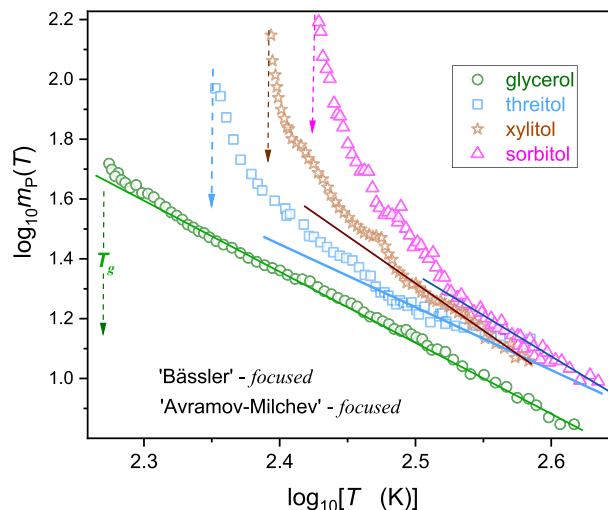


Fig. 4. Distortion-sensitive plot focused on searching domains, preferably described by the AM [60] Eq. (22): straight lines indicate them.

scaling relations, for instance:  $(\tau(T)/\tau_0)^{-1/\phi}$  vs  $T/T_C$  for the critical-like Eq. (27) [62,68],  $\log_{10}\tau$  vs  $A_{VFT}/(T-T_0)$  for VFT Eq. (3) [17,67,100,101],  $\log_{10}\tau$  vs  $A_{AM}/T^D$  for AM Eq. (21) [60]. One may also propose a plot for MYEGA Eq. (12):  $T\log_{10}\tau$  vs  $C \ln(K/T)$ . In each case, such scaling plots *a priori* lead to overlapping all used experimental data, if only the given relation may effectively portray results data within the limits of experimental errors. Hence, such multiple-scaled plots cannot be considered valid for a given model relation.

Fig. 5 shows that for a member of tested series of polyols, changes of  $m_p(T)$  are strongly non-linear, including glycerol, for which an additional test is shown in the inset. Following Eq. (21) the results presented in Fig. 5 show the fundamental inadequacy of ‘parabolic’ CGE Eq. (23) [66,111–113] for portraying previtreous dynamics in glycerol, threitol, xylitol, and sorbitol.

As mentioned above, the VFT Eq. (3) may be considered as dominant relation for portraying previtreous dynamics. It can be alternatively presented using the fragility:

$$\log_{10}\tau(T) = \log_{10}\tau_\infty + \frac{\zeta^2}{m(T/T_g - 1) + \mu} \tag{25}$$

where  $\zeta = m\log_{10}\tau(T_g)\log_{10}\tau_{\infty min}$ .

The comparison of Eqs. (3) and (25) yields the link:  $D_T = T_g m_{min}^2/m$  and  $T_0 = T_g(1 - m_{min}/m(T/T_g - 1))$ .

For VFT relation, one may derive the following linearized equation [102]:

$$\frac{d\ln\tau(T)}{d(1/T)} = -T^2 \frac{d\ln\tau(T)}{dT} = \Phi \left( \frac{T}{T - T_0} \right)^2 \tag{26}$$

where  $\Phi = D_T T_0$  and  $d\ln\tau(T)/d(1/T) = H'_a(T) = H_a(T)/R$ ;  $H_a(T)$  is for the apparent activation enthalpy, and  $R$  means the gas constant.

The above relation directly yields the linearized equation [102]:

$$\left[ \frac{d\ln\tau(T)}{d(1/T)} \right]^{-1/2} = [H'_a(T)]^{-1/2} = (D_T T_0)^{-1/2} - T_0 (D_T T_0)^{-1/2} \times \frac{1}{T} = -A \frac{1}{T} + B \tag{27}$$

Note the direct link to the ‘Stickel operator’ [93]  $\phi_T = d\log_{10}\tau(T)/d(1/T)$  introduced for determining the dynamic crossover temperature  $T_B$ , and the apparent fragility:

$$\left( \frac{d\ln\tau(T)}{d(1/T)} \right)^{-1/2} = [H'_a(T)]^{-1/2} = (T_g \ln 10)^{-1/2} [m_p(T)]^{-1/2} = \frac{1}{\sqrt{\ln 10}} \phi_T(T) \tag{28}$$

The comparison of Eqs. (27) and (28) explicitly show that the broadly applied ‘Stickel analysis’ [93] is based on the assumption that both the lower and upper fragility are described by the VFT Eq. (3), but with a different set of parameters:  $D_T$  related to fragility and the singular temperature  $T_0$ . All of these led to the ‘virtual’ glass temperature for the upper dynamic domain and the real dynamic domain in the lower dynamic domain. Eq. (27) also indicates the possibility of an alternative plot:

$$T[H'_a(T)]^{-1/2} = (D_T T_0)^{-1/2} \times T - T_0 (D_T T_0)^{-1/2} = AT - B$$

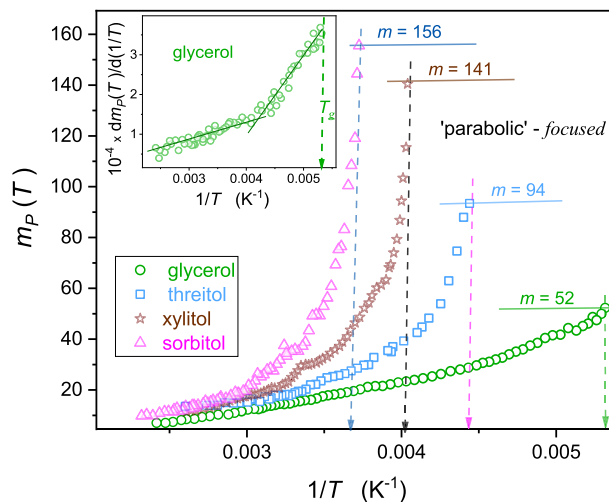


Fig. 5. Temperature evolution of apparent fragility (steepness index), in polyols, using scale correlated to Angell plot and Eq. (22). The latter is focused on testing the preference for CGE description [57]: such domains should follow a linear pattern. The inset presents derivative data from the central part of the plot, indicating that evolution  $m_p(1/T)$  is not linear for glycerol.

Alternative plots  $[d \ln \tau(T)/d(1/T)]^{-1/2} [H_a'(T)]^{-1/2}$ ,  $[m_p(T)]^{-1/2}$  or  $\phi_T(T)$  vs  $1/T$  or alternatively  $T \times [H_a'(T)]^{-1/2}$ ,  $T \times [m_p(T)]^{-1/2}$  vs  $T$  should yield the linear behavior for the validated description of experimental data by the VFT relation. Linear regression fit can yield parameters  $A$  and  $B$ , and then:  $D_T = 1/AB$  and  $T_0 = B/A$ .

As mentioned above, in high-temperature dynamic domains of supercooled systems, critical-like portrayal within the MCT approach is advised [68,97,98]. The same type of portraying was considered for the low-temperature dynamic domain, close to the glass temperature:

$$\tau(T) = \tau_0(T - T_C)^{-\varphi}, \quad \tau(T) = \tau_0 \left( \frac{T - T_C}{T_C} \right)^{-\varphi} \tag{29}$$

$$\tau(T) = \tau_0 \left( \frac{T - T_C}{T} \right)^{-\varphi} \tag{30}$$

where  $T \geq T_g$ ,  $T_C < T_g$ . For dynamic critical phenomena [114]:  $\varphi = z\nu$ ;  $\nu$  and  $z$  is exponents for correlation length  $\xi$ , and  $z$  is a dynamic exponent.

Four decades ago, Souletie and Bertrand conducted comparative tests of such descriptions for several systems [115,116]. Unfortunately, their results show the non-conclusive scatter of the exponent  $\varphi$  and a relatively poor-fitting quality. Saltzmann and Schweitzer [117] analyzed a hypothetical critical universality numerically in polymeric glass formers and suggested  $\varphi \approx 1.7$ . Experimental validation of these results in low molecular weight liquids seems doubtful [115–117]. Two decades ago, Colby [63,64] announced hypothetically breakthrough results, indicating universal and critical-like behavior by Eq. (29) with the universal exponent  $\varphi = z \times \nu = 6 \bullet 3/2 = 9$ , supported by validating evidence for 35 glass-forming systems [63]. The exponential multiplier was advised for some molecular liquids [64]. Heuristic considerations supporting this reasoning were called the ‘dynamic scaling model’ (DSM) [63,64]. However, this result has been skeptically treated even for the same experimental datasets as in ref. [63,64] declared universal DSM criticality was not confirmed [62].

Authors of this report developed the linearized distortions-sensitive analysis for the critical-like Eq. (19) [102]:

$$\frac{T^2}{H_a'} = \frac{T_C}{\varphi} - \varphi^{-1}T = A - BT \tag{31}$$

Using a plot  $T^2/H_a'(T)$  vs  $T$ , linear behavior shows domains where Eqs. (29) and (31) can be applied; subsequent linear regression yields basic parameters:  $T_C = AB$  and  $\varphi = 1/B$ .

In refs. [38,55,99,118–122] the linearized distortion-sensitive analysis was applied for liquid crystalline glass-formers composed of rod-like molecules, showing a clear prevalence for critical-like portrayal with the exponent  $\varphi = 9$ . Hence, behavior suggested by DSM approach appears, although not in systems indicated in basic DSM refs. [63,64]. The prevalence of the critical-like portrayal was also found in plastic crystals and some low-molecular-weight liquids and polymers where local elements of uniaxial symmetry occur [55,99,105].

Figs. 6 and 7 present results of linearized, the derivative-based analysis focused on VFT (Eq. (3)) and the critical-like (Eq. (31)) scaling of pre-vitreous dynamics. Distortion-sensitive analysis reveals that near  $T_g$  VFT portrayal obeys only glycerol. Such a behavior ceases to be optimal when shifting from glycerol to sorbitol in a homologous series, as visible by emerging non-linearity. A reversed behavior occurs when testing critical-like portrayal preference (Eq. (31)). It is optimal for sorbitol and becomes non-optimal when

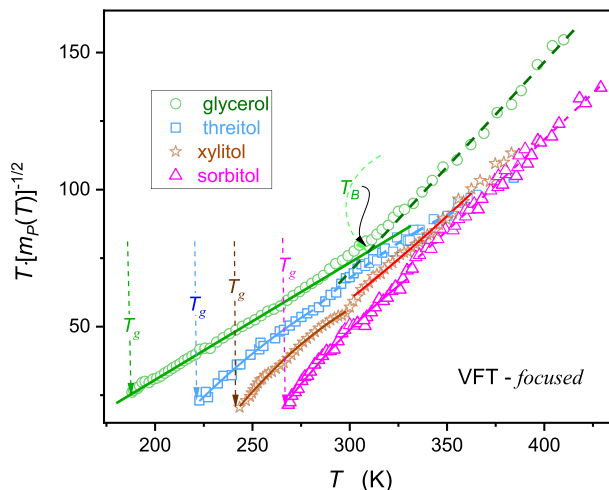


Fig. 6. Distortion-sensitive plot (Eq. (27)) focused on searching domains, preferably described by VFT description Eq. (3); straight lines indicate them. The presentation is equivalent to the Stickel et al. [93] plot introduced for detecting the dynamic cross-over temperature  $T_B$ .

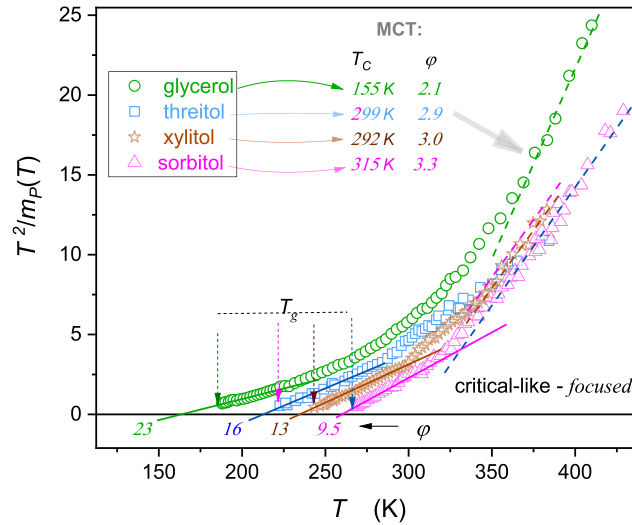


Fig. 7. Distortion-sensitive plot focused on searching domains, preferably described by the critical-like description Eq. (31): straight lines indicate them.

shifting from sorbitol to glycerol in the tested series, as visible in Fig. 7. Notable that for sorbitol, which molecule shows the ‘strongest’ uniaxial features, the exponent  $\phi \approx 9.5$  for  $T \rightarrow T_g$ . Such a value is approximately the same as in rod-like liquid crystalline glass-formers [118–122] and roughly the same as introduced by Colby within the Dynamical Scaling Model [63,64]. In the high-temperature domain, well above  $T_g$ , the second critical-like domain emerges (Fig. 7), in agreement with the MCT approach expectations for HT ergodic part of the previtreous domain. The plot also shows the values of MCT [68,97,98] exponents ‘critical’ temperatures in the high-temperature dynamic domain. Regarding the low-temperature domain near  $T_g$  the following parameters have been obtained: (i) for glycerol  $T_C = 155K$  and  $\phi \approx 23$ , (ii)  $T_C = 214K$ ,  $\phi \approx 16$  for threitol, (iii) for xylitol  $T_C = 233K$  and  $\phi \approx 13$ , (iv)  $T_C = 254K$ ,  $\phi \approx 9.5$  for sorbitol. The latter extends up to ca.  $T_g + 50K$ .

Recently, one of the authors (ADR) showed the common pattern empirically for the evolution of the apparent fragility for ten glass formers, covering low molecular weight liquids, liquid crystals, plastic crystals, polymers, and resins [99]:

$$m_P(T) = \left. \frac{d \log_{10} \tau(T)}{d(T_g/T)} \right|_{T > T_g} = \frac{A}{T - T_g^*} \tag{32}$$

The extrapolated singular temperature  $T_g^* < T_g$  may be simply determined from the condition  $1/m_P(T_g^*) = 0$ . Linking the above empirical equation with the definition of apparent fragility, one obtains the differential equation, which solution leads to the following scaling dependence for the previtreous behavior [99]:

$$\tau(T) = C_\Gamma \left( \frac{T - T_g^*}{T} \right)^{-\Gamma} \left[ \exp \left( \frac{T - T_g^*}{T} \right) \right]^\Gamma = C_\Gamma (t^{-1} \exp t)^\Gamma \tag{33}$$

where  $t = (T - T_g^*)/T$

The power exponent can be expressed via basic empirical metrics of the glass transition:  $= m \ln 10 (T_g/T_g^*) / (1/(\Delta T_g^*/T_g) - 1)$ ,

Table 1

Values of parameters for the AC Eq. (33).  $T_g^*$ ,  $\Gamma$ ,  $C_\Gamma$  are for the low-temperature (LT) dynamic domain. Parameters for the high-temperature (HT) dynamic domain are denoted as  $T_B^*$ ,  $\Gamma_B$ ,  $C_{\Gamma B}$ , and related numbers are in *italic*.

Glass-former	$T_g(K)$	$T_g^*(K)$ $T_B^*$	$\Gamma$	$\log_{10} C_\Gamma \log_{10} C_{\Gamma B}$
Glycerol	186.0	147.0.1	34.3	-19.48
		225.1	7.05	-13.31
Threitol	224.2	200.4	19.3	-17.47
		270.1	4.7	-12.6
Xylitol	247.6	231.5	16.02	-17.08
		299.3	4.1	-12.6
Sorbitol	267.0	259.1	11.4	-15.33
		300.1	3.85	-12.7

$\Delta T_g^* = T_g - T_g^*$ . The unique feature of Eq. (33) is the ‘activation-critical’ (AC) formula linking critical-like and activation (SA-type) features. The value of the exponent determines their relative share in the previtreous effect. The parallel relation may be introduced for the high-temperature dynamic domain. In this case, the singular temperature  $T_B^* < T_B$  and the power exponent  $\Gamma_B$  replace parameters in Eqs. (31).

Emerging from the comparison of Figs. 6 and 7, interplays between activation-type (SA) and critical-like (CL) dynamics indicate ‘mixed’ scaling as a possible optimal parameterization for the homologous series of tested polyols. Such a relation (Eq. (31)) has been introduced recently and validated for a set of glass-forming systems [86].

Values of parameters are collected in Table 1. It is worth noting that values of singular temperatures  $T_g^*$  and  $T_B^*$  may be readily determined before the fitting of  $\tau(T)$  experimental data by analysis, which results are shown in Fig. 8. This causes a final fit of  $\tau(T)$  can be limited only to two parameters. Values of parameters given in Table 1 show that the power exponent in Eq. (33) is responsible for the relative impact of the critical-like and activation contributions to the previtreous effect.

Finally, returning to ‘extended’ VFT-type relation, related to DDM Eq. (16) and OIM Eq. (17) checkpoint relations. As for Eq. (16) one can consider the following derivative-based transformation:

$$\begin{aligned} \frac{d \ln \tau(T)}{dT} &= -\theta \Phi (T - T_0)^{-\theta-1} = \frac{T_g \ln 10}{T^2} \frac{d \log_{10} \tau(T)}{d(T_g/T)} = \frac{T_g \ln 10}{T^2} m_P(T) \Rightarrow \theta = 3/2 \Rightarrow \\ \Rightarrow \left[ \frac{d \ln \tau(T)}{dT} \right]^{-5/2} &= \frac{T_g \ln 10}{T^2} = \frac{T^3}{(T_g \ln 10)^{5/2}} (m_P(T))^{-5/2} = AT - B \end{aligned} \tag{34}$$

where  $A = \theta \Phi$ , and  $B = T_C \theta \Phi$ .

The analysis of experimental data based on the plot  $(m_p)^{-5/2}$ , or alternatively  $(H'_a)^{-5/2} = (d \ln \tau / d(1/T))^{-5/2}$  vs  $T$  yielded linear dependences less pronounced than for the VFT or MYEGA relations discussed above.

The unique functional modification of the references introduces the OIM related VFT2 Eq. (17). The functional form of this dependence suggests the following derivative-based linearized relation:

$$\frac{d \ln \tau(T)}{d(T_C/T)} = \frac{1}{C} (T - T_C)^{-3} \Rightarrow \left[ \frac{d \ln \tau(T)}{d(T_C/T)} \right]^{-1/3} = C^{1/3} T - C^{1/3} T_C = AT - B \tag{35}$$

The plot defined by Eq. (35) was used in ref. [92] for testing the validity of OIM Eq. (17). It was carried of for glycerol, propylene glycol (PG), polyvinyl acetate (PVAc), propylene carbonate (PC), sorbitol. For PVAc, Sorbitol, and particularly PC, the analysis revealed a strong distortion from linearity when cooling towards  $T_g$ , was explained as the impact of the VFT4 term. The supplementary fit of  $\tau(T)$  experimental data via VFT Eq. (3), MYEGA Eq. (12), and (OIM) Eq. (17) showed the prevalence of the latter via the slightly smaller coefficient  $\chi^2$  showing the normalized mean square of the deviation between experimental data and portraying function.

Notable that Eq. (17) requires the knowledge of the OIM ‘critical’ temperature in prior, which can be determined, for instance, using  $(d \ln \tau(T) / d(1/T))^{-3}$  s. vs  $T$  plot. Fig. 9 shows the derivative-based linearized test of the OIM Eq. (17) scaling relation for the homologous series of tested polyols using the following parallel of Eq. (35):

$$\left[ \frac{T_g}{T_C} \frac{d \ln \tau(T)}{d(T_g/T)} \right]^{-1/3} = \left( \frac{T_g}{T_C} \right)^{-1/3} (m_P(T))^{-1/3} \Rightarrow (m_P(T))^{-3} = A'T - B' \tag{36}$$

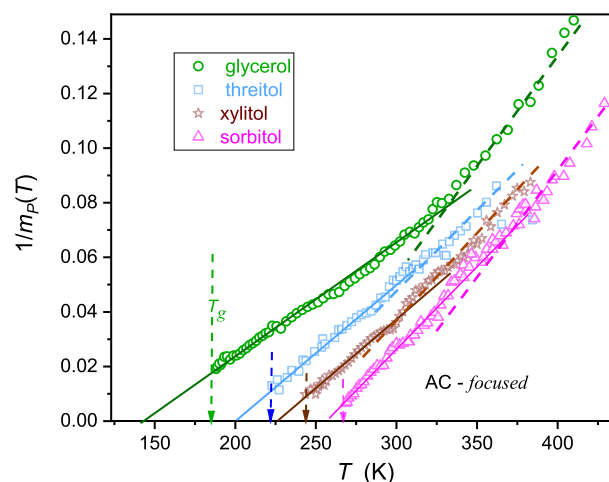


Fig. 8. Pre-vitreous universal changes of the apparent fragility in the pre-vitreous domain of polyols emerging due to for  $1/m(T)$  vs  $T$  plot. Arrows indicate glass temperatures. Linear behavior is linked to Eq. (32).

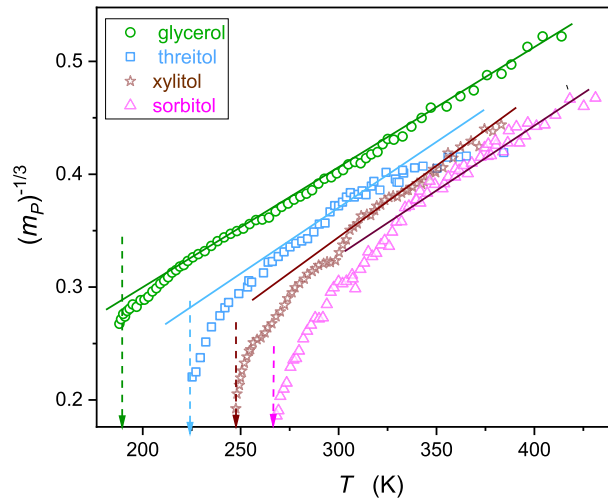


Fig. 9. The linearized derivative-based test (Eq. (36)) of the ability of the OIM Eq. (17) for portraying previtreous dynamics in the homologous series of polyols. The ‘validated domain’ is indicated by linear behavior.

where  $A = C^3(T_C/T_g)^{1/3}$ ,  $B = T_C(T_C/T_g)^{1/3}$ . The singular (‘critical’) temperature is determined from the extrapolation of the linear down to  $(m_P(T))^{-1/3} = 0$ .

In ref. [92] OIM Eq. (17) was validated via the above derivative-based plot, which enables a convenient estimation of the singular temperature and the comparison of  $\chi^2$  values for portraying experimental  $\tau(T)$  data via VFT, MYEGA, OIM scaling relations. Tests were carried out in the previtreous domain of glycerol, sorbitol, polyvinyl acetate, propylene glycol, and propylene carbonate.

Fig. 9 shows that OIM Eq. (17) is able to portray only dynamics in the high temperature dynamic (HT) domain, and even in the given case, this domain shrinks when shifting from glycerol to sorbitol. When entering the LT dynamic, the portrayal via Eq. (17) fails, as shown by significant nonlinear changes. In ref. [ ] such distortions were explained by the rising impact of VFT4 term. However, taking this factor into account increases the number of fitted parameters.

## 5. Activation energy index for analysis previtreous dynamics

Hecksher et al. [53] proposed to focus on the activation energy index introduced by Dyre and Olsen [43]:  $I_{DO}(T) = -d \ln E_a(T) / d \ln T = (dE_a/E_a) / (dT/T)$ , i.e., to transform experimental data  $\tau(T) \rightarrow I_{DO}(T)$ . The required apparent activation energy was calculated from general SA Eq. (1),  $E_a(T) = RT \ln(\tau(T)/\tau_\infty)$  assuming the universal value of  $\tau_\infty$ . In ref. [53] the analysis of 42 low-molecular-weight glass formers led to the conclusion: ‘...there is no compelling evidence for the Vogel–Fulcher–Tammann (VFT) prediction that the relaxation time diverges at a finite temperature. We conclude that theories with a dynamic divergence of the VFT form lack a direct experimental basis.’

It was formulated by comparing experimental  $I_{DO}(T)$  evolutions with model  $I_{DO}(T)$  dependences for the VFT relation and two proposed functions without finite temperature singularities (denoted as FF1 and FF2 in ref. [53]). In subsequent years, ref. [53] has become an inspiration for developing theoretical models avoiding finite temperature singularities below  $T_g$ . However, the pre-exponential factor assumption regarding the universal, constant value  $\tau_\infty = 10^{-14}$ s in ref. [53], poorly correlate with experimental evidence and may lead to a bias for calculated values of  $E_a(T)$  and then  $I_{DO}(T)$ . In ref. [55] protocol avoiding this problem was proposed: apparent activation energy was calculated as a solution of differential equation resulting from SA Eq. (1) or the selected set of  $\tau(T)$  experimental data:

$$R \frac{d \ln \tau(T)}{d(1/T)} = \frac{1}{T} \frac{dE_a(T)}{d(1/T)} + E_a(T) \quad (37)$$

In Eq. (34)  $d \ln \tau / d(1/T) = H_a^*(T) = H_a(T)/R$ , where  $H_a(T)$  is the apparent activation enthalpy. As results from Eq. (34)  $H_a(T) \neq E_a(T)$  for the SA dynamics. In refs. [55–57] the analysis exploring Eq. (34) for determining the apparent activation energy was applied for 26 glass formers, ranging from low-molecular-weight liquids, polymers, plastic crystals to liquid crystals. The common ‘universal’ pattern of the index was found:  $1/I_{DO} = a + bT$ . Subsequently, a hypothetical general formula for activation energy index was found [56,57]:

$$I_{DO}(T) = nT_0 / (T - T_0) = \frac{nT_0}{T - T_0} \quad (38)$$

It was concluded from  $I_{DO}(T)$  derived form for VFT, Avramov-Milchev (AM), MYEGA, and critical-like (CL) dependences [45]. The study of experimental data in refs. [55,123] showed that  $0.18 < (n = -1/a) < 2.2$ . VFT portrayal appears for systems characterized by

$n = 1$  with orientational, uniaxial ordering, whereas  $n \approx 0.18$  for systems with translational symmetry. Notably, for MYEGA [59] equation  $a = 0$ , and the Avramov-Milchev (AM) [0] dependence  $b = 0$  and then  $1/I_{DO}(T) = \text{const}$ . For VFT and CL scaling relations:  $a \neq 0$  and  $b \neq 0$ .

Elmatad et al. [66] considered a parabolic scaling plot of activation energy defining a cross-over temperature  $T_o > T_m$ , and  $J$  is a parameter setting the excitation energy [59]. The activation energy for this scaling approach can be written as:

$$E_a(T) = \left(\frac{J}{T_o}\right)^2 T \left(\frac{T_o}{T} - 1\right)^2, \text{ for } T < T_o \tag{39}$$

Consequently, the following formula for the activation energy index is obtained:

$$I_{DO}(T) = \frac{T + T_o}{T - T_o} \tag{40}$$

Reciprocal of the index does not follow linear behavior and exhibits an artificial anomaly associated with an onset temperature  $T_o$ , related to the crossover between Arrhenius and Super-Arrhenius dynamics domains in the high-temperature region.

A similar disagreement with experiment occurs for Roessler et al. [88] Eq. (15), for which the derived index is given in Table 2.

Notable is the relation links apparent activation energy, activation energy index, and configurational entropy derived in Refs. [45,120] is:

$$I_{DO}(T) = \frac{1}{T} \frac{d \ln E_a}{d(1/T)} = - \frac{1}{TS_C(T)} \frac{dS_C(T)}{d(1/T)} \tag{41}$$

By applying the experimental evidence for apparent activation energy index evolution (Eq. (35)) one obtains the following relation for previtreous changes of configurational entropy [55]:

$$S_C(T) = S_0 \left(1 - \frac{T_0}{T}\right)^n = S_0 t^n \tag{42}$$

where  $t = (T - T_0)/T$ .

It is worth stressing that the essential difference between Eq. (39) and the ‘classic’ Eq. (9), associated with  $n = 1$  and  $T_0 = T_K$ , and leading to VFT Eq. (3) after the substitution to Adam-Gibbs model Eq. (7). Eq. (39) is related to  $n \neq 1$ . The functional form of Eq. (42) resembles the behavior observed for Critical Phenomena. This link is strengthened by the empirical correlation between ‘ $n$ ’ values and the local symmetry of the system. Particularly worth stressing is the value  $n \approx 3/2$  detected in glass forming rod-like liquid crystalline compounds. In the given case, the local uniaxial molecular symmetry is matched with the lack of translational symmetry. On the other hand, in orientationally disordered crystals (ODICs)  $n \approx 0.18$  [55,120]. In the given case, the translational ordering is linked to the orientational freedom. Worth stressing is the empirical correlation between the singular temperature  $T_0$  and the Kauzmann temperature  $T_K$  [46] Such correlation is limited for  $n = 1$ . Moreover, the behavior described by Eq. (42) extends in the low-temperature (ultraviscous, ultraslow) dynamical domain extending up to  $T_g + 80K$  [42]. Substituting Eq. (42) to the basic AG model relation (Eq. (7)), one obtains the extended VFT following dependence:

$$\tau(T) = \tau_\infty \exp\left(\frac{DT^{n-1}}{(T - T_0)^n}\right) = \tau_\infty \exp\left(\frac{D/T}{t^n}\right) \tag{43}$$

where  $D = A\Delta\mu/S_0$ .

For  $n = 1$  Eq. (40) converts into basic VFT Eq. (3), and then  $D = D_T$ ,  $T_0$  is the VFT singular temperature. Extended VFT Eq. (43) with  $n \neq 1$  was independently introduced to portray previtreous dynamics in polyvinylidene disulfide (PVDF) and BST ferroelectric microparticles [124] as well as for relaxor ceramics [125]. Formally, Eq. (43) is associated with four fitted parameters, but values of  $n$  and  $T_0$  may be estimated from activation energy index analysis or heat capacity data. It is worth stressing, that the emerging similarity of Eq. (43) and RFOT model [85] general relation (Eq. (10)). The latter can be retrieved if the power exponent  $n = \alpha = \psi/(d - \theta)$ .

It is notable that Eq. (43) for  $\tau(T)$  evolution was obtained assuming configurational entropy derived from  $\tau(T)$  experimental data expressed by Eq. (42). Crucial validation requires obtaining behavior described by Eq. (42) from thermodynamic data analysis. At first sight, the credibility of Eq. (41) seems to be doubtful since experimental confirmation of classic Eq. (9), linked to  $n = 1$ , is very extensive [49,54,67,70,75,78]. Notwithstanding, analysis based on non-linear fitting of experimental data remote from singular Kauzmann temperature  $T_K$ . The very recent report [110] copes with this essential feature of previtreous behavior for glass transitions, analyzing high-resolution experimental data for 8 glass-forming systems via the following distortions-sensitive approach for Eq. (39):

$$\ln S_C(T) = \ln S_0 + n \ln \left(1 - \frac{T_K}{T}\right) \Rightarrow \frac{d \ln S_C}{d(1/T)} = \frac{n T_K}{1 - T_K/T} \tag{44}$$

Consequently, one obtains the following linear behavior validating Eq. (39) for the plot defined by the following relations:

$$\left[\frac{d \ln S_C(T)}{d(1/T)}\right]^{-1} = \frac{1}{n T_K} - \left(\frac{1}{n}\right) \left(\frac{1}{T}\right) = A + B \left(\frac{1}{T}\right) \tag{45}$$

Figs. 10 and 11 show the results of such analysis for glycerol and propanol. Table 3 below presents the summary of results discussed

**Table 2**

Basic model relation and related forms of reciprocal of the activation energy index, including the corresponding parameter 'n'. The experimental evidence is also summarized.

Theory/Models	Model Equation	1/I <sub>Do</sub>	Parameter n
	VFT: $\tau(T) = \tau_{\infty} \exp\left(\frac{D_T T_0}{T - T_0}\right)$	$\left(\frac{1}{T_0}\right) T^{-1}$	1
	MYEGA: $\tau(T) = \tau_{\infty} \exp\left[\frac{C}{T} \exp\left(\frac{K}{T}\right)\right]$	$\left(\frac{1}{C}\right) T$	0
	AM: $\tau(T) = \tau_{\infty} \exp\left(\frac{A_{AM}}{T^D}\right)$	$\frac{1}{D-1}$	undefined
	Critical-like: $\tau(T) = \tau_{\infty} (T - T_C)^{-\varphi}$	$\left(\frac{1}{\varphi}\right) T - \frac{T_C}{\varphi}$	~ 0.2 (PC)~1.5 (LC)
	CGE: $\tau(T) = \tau_{\infty} \exp\left[C\left(\frac{1}{T} - \frac{1}{T_0}\right)^2\right]$	$\frac{T - T_0}{T + T_0}$	undefined
	Roessler et al. [ ]: $\tau(T) = \tau_{\infty} \exp\left[\frac{E_{\infty} + a \exp(-\lambda(T/T_A - 1))}{T}\right]$	$\frac{T/T_A}{1 + \exp[\lambda(T/T_A - 1)]}$	undefined
Experiment: $1/I_{Do} = aT + b, n = -1/b$ (PC: critical-like) $\Leftarrow 0.18 < n < 2.2 \Rightarrow$ (LC: critical-like) $n = 1$ (SA: VFT)			

in ref. [124]. These results support the generalized Eq. (42) for the configurational entropy, with the exponent  $n \neq 1$ , within frames indicated by ref. [124].

Fig. 10 shows that direct portrayals of  $S_C(T)$  experimental data for  $T > T_g$  via discussed dependences, associated with  $n \neq 1$ , and  $n = 1$ , yields almost indistinguishable fitting qualities, particularly when including the impact of the experimental error. Notwithstanding, the generalized relation for configurational entropy evolution (Eq. (42)) yields notable correction in the estimation of the Kauzmann temperature, as shown in Fig. 11 and ref. [124].

As a general comment for the analysis exploring activation energy index for relaxation, one should note that it applies the second and even the third-order derivative of  $\tau(T)$  experimental data, supported by numerical filtering using the Savitzky-Golay principle [55]. All of these introduce some degree of uncertainty to results.

**6. Distortion-sensitive tests of previtreous dynamics under pressure**

Isothermal compressing constitutes an alternative way of approaching the glass transition. Relation to describe pressure-viscosity behavior was firstly proposed by Barus (B) in 1893, via the relation  $\eta(P) \propto \exp(\alpha P)$ ,  $\alpha = const$  [126]. Nowadays, this relation is used in the super-Barus (SB) form, with a pressure-dependent coefficient  $\alpha(P)$ :

$$\tau(P) = \tau_{\infty}^T \exp(\alpha(P) \times P) = \tau_{\infty}^T \exp\left(\frac{V_a(P)}{RT} P\right) \tag{46}$$

where  $T = const$ ,  $P < P_g$  and  $P_g$  is for glass (vitrification) pressure;  $V_a(P)$  denotes apparent activation volume.

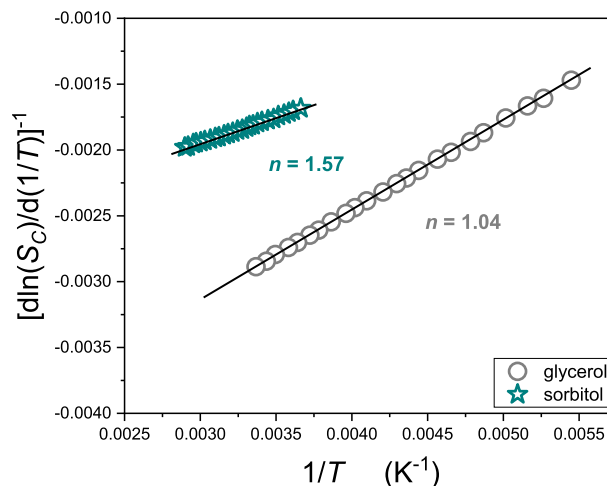


**Fig. 10.** The derivative-based analysis of configurational entropy (Eq. (42)) for two selected supercooled liquids focused on testing new relation  $S_C(T)$  behavior, given by Eq. (41).

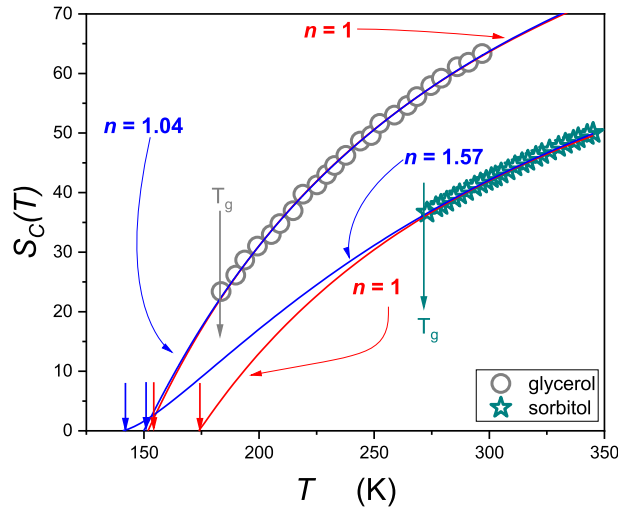


**Fig. 11.** Temperature dependences of configurational entropy in glycerol and sorbitol. In red, the description classic description by Eq. (9), alternatively Eq. (42) with parameter  $n = 1$  are shown. In blue fitting via Eq. (42) with parameters  $n \neq 1$ , derived in Fig. 10, is presented.

**Table 3**

Values of parameter  $n$  reported in ref. [110] using the derivative-based analysis via Eq. (42).

System	Sorbitol	8*OCB (LC: rod-like)	Ethanol	Glycerol	Diethyl phtalate	Cycloheptanol (PC: ODIC)
$n$	1.57	1.51	1.28	1.04	0.98	0.18

Note that in both Barus (B) and Super-Barus (SB) equations, the pre-exponential factor:

$$\tau_{\infty}^T = \tau(P = 0) \approx \tau(P = 0.1MPa) \tag{47}$$

Williams introduced the activation volume into this relation in 1964 [75,76], as follows:

$$V_a = RT \frac{d \ln \tau(P)}{dP} \tag{48}$$

where  $V_a(P) = V_a = const$  in the given pressure domain, related to the basic Barus relation. The latter equation is not valid for pressure-dependent apparent activation volume, i.e., for the SB dynamics:

$$RT \frac{d \ln \tau(P)}{dP} = V_a(P) + P \frac{dV_a}{dP} \tag{49}$$

and consequently

$$V^{\#}(P) = RT \frac{d \ln \tau(P)}{dP} \neq V_a \tag{50}$$

Taking into account the definition of pressure-related apparent fragility (steepness index) defined below, one may show that  $V^{\#}(T) \propto m_T(P)$ . The general Super-Arrhenius and Super-Barus relation may be obtained by linking Eqs. (1) and (46) [127]:

$$\tau(T, P) = \tau(T) \tau(P) = \tau_{ref} \cdot \exp\left(\frac{E_a(T) + PV_a(P)}{RT}\right) \tag{51}$$

where  $T > T_g$  and  $P < P_g$ . A similar relation occurs for  $\eta(T, P)$  changes.

Following eq. (51), an isobaric temperature evolution is described by:

$$\tau(T) = \left[ \tau_{\infty}^T \exp\left(\frac{PV_a(P)}{RT}\right) \right] \exp\left(\frac{E_a(T)}{RT}\right) = \tau_{\infty}^P \exp\left(\frac{E_a^P(T)}{RT}\right) \tag{52}$$

Eq. (48) correlates with SA Eq. (1) for  $P = 0$ . Such an isobar may be approximated by temperature studies under atmospheric pressure ( $P \approx 0.1MPa$ ). Eq. (48) shows a pattern of changes in pre-exponential factor when carrying out temperature tests under higher pressures.

For isothermal pressure-related previtreous behavior, plot  $\log_{10} \tau(P)$  or  $\log_{10} \eta(P)$  vs  $P/P_g$  is often indicated as a possible pressure

counterpart of the Angell plot. However, such a presentation of data leads to a gamut of curves instead of a compact representation characterizing a temperature-related Angell plot. The mentioned normalized  $\tau(P)$  or  $\eta(P)$  evolutions lead to the following pressure-related steepness index (apparent fragility) [128,129]:

$$m_T(P) = \frac{d \log_{10} \tau(P)}{d(P/P_g)}, \quad m_T = m_T(P \rightarrow P_g) \tag{53}$$

where  $m_T$  denotes pressure-related fragility metric. The above yields  $\mu_p = \log_{10} \tau(P_g) - \log_{10} \tau_\infty^P$  for the minimal fragility characterizing the basic Barus dynamics: fragility. However, depending on the tested isotherm, it may range from 1 to even 14. It is also notable that Eqs. (48) and (49) lead to the ‘artificial’ anomaly of apparent fragility for  $P \rightarrow 0$  [128,129]. All above indicates significant inconsistencies in the general characterization of the previtreous effect in super-compressed liquids.

Similar to basic SA Eq. (1) and SB Eq. (43) does not enable the portrayal of experimental data due to an unknown form of an evolution of apparent activation volume. Consequently, replacement relations are necessary. In 1972 Johari and Whalley (JW) applied the following empirical dependence for portraying experimental data in super-compressed glycerol ( $T = 20^\circ\text{C}$ ) [130]:

$$\tau(P) = \tau_\infty^T \exp\left(\frac{J}{P_0 - P}\right) \tag{54}$$

where  $J = \text{const}$ ,  $P < P_g$ , extrapolated singular pressure  $P_0 > P_g$ .

However, this relation may reliably portray experimental data only if they are relatively close to the basic Arrhenius/Barus pattern (i.e., ‘strong’ glass-formers) or in a ‘narrow’ range of pressures. Moreover, it cannot be reduced to basic Barus equations with  $V_a(P) = V_a = \text{const}$ , an essential feature required for any SB replacement scaling relation. When comparing general SB Eq. (46) and JW Eq. (54) a significant inconsistency also occurs for the pre-exponential factor: in Eq. (54)  $\tau_\infty^T \neq \tau(P = 0)$ . In 1998, an application of new BDS facilities and designs of measurement capacitors placed within pressure chambers enabled obtaining the high-resolution  $\tau(P)$  experimental data for ultraviscous glycerol compressed up to 0.35 GPa for  $T = 260\text{K}$ , showing the explicit fragile behavior. Analysis showed limited adequacy of Eq. (50) and the fair portrayal by an empirical relation [131]:

$$\tau(P) = \tau_\infty^T \exp\left(\frac{J(P)}{P_0 - P}\right) = \tau_\infty^T \exp\left(\frac{D_p P}{P_0 - P}\right) \tag{55}$$

It can fair portray dynamics for both ‘strong’ and ‘fragile’ glass-formers. It also introduced the fragility strength coefficient  $D_p$  for a pressure path. Notably, it may be reduced to the basic Barus equation and the prefactor  $\tau_\infty^T = \tau(P = 0)$ , as in basic Barus and Super-Barus relations (Eq. (43)). It also can be derived from the VFT Eq. (3) by a simple substitution  $T = \delta/P$ , and  $\delta = \text{const}$ , i.e., the basic qualitative link between cooling and compressing:

$$\tau(T) = \tau_\infty \exp\left(\frac{D_T T_0}{T - T_0}\right) \Rightarrow \tag{56}$$

$$\tau_\infty^T \exp\left[\frac{D_T(\delta/P_0)}{\delta/P - \delta/P_0}\right] = \tau_\infty^T \exp\left[\frac{D_T(\delta/P_0)}{\delta(1/P - 1/P_0)}\right] = \tau_\infty^T \exp\left[\frac{D_T(\delta/P_0)}{\delta\left(\frac{P_0 - P}{P_0 P}\right)}\right] = \tau_\infty^T \exp\left[\frac{D_T P}{P_0 - P}\right]$$

Notwithstanding, in a new PVFT Eq. (55), the problem of pre-exponential factor inconsistency, characterizing SB Eq. (46), remains. It may be solved, considering that liquids or solids can be isotopically stretched, which is equivalent to negative pressures, and passing  $P = 0$  without any hallmark [132,133]. The stretching is possible until an absolute stability limit spinodal  $P_{SL} < 0$ , where intermolecular interactions break, is reached. Experimental evidence of smooth passing from the ‘positive’ to the ‘negative’ pressure domains in glass-forming liquids was shown by Angell and Quing [134]. All these led to generalized SB and PVFT relations [110]:

$$\tau(P) = \tau_\infty^T \exp\left(\frac{V_a(P)}{RT} \Delta P\right) \tag{57}$$

$$\tau(P) = \tau_\infty^T \exp\left(\frac{D_p^{SL}(P - P_{SL})}{P - P_0}\right) = \tau_\infty^T \exp\left(\frac{D_p^{SL} \Delta P}{P - P_0}\right) \tag{58}$$

where  $D_p^{SL}$  is fragility strength corrected by the impact of stability limit (SL) pressure and  $\Delta P = P - P_{SL}$ .

Note that Eq. (57) resembles the one proposed by Kieβkalt yet in 1927 [135]:  $\eta = \eta_0 e^{a(P-P_0)}$ . but  $P_0$  was referred to as some ‘characteristic positive’ pressure, and the negative pressures domain was not considered there. Eqs. (57) and (58) directly lead to the plot  $\log_{10} \tau(P)$  vs  $\Delta P = P - P_{SL}$  as the pressure counterpart of Angell plot, see ref. [110]. It is worth noting that Eqs. (57) and (58) are associated with similar values of prefactor  $\tau_\infty^T \neq \tau(P_{SL}) \cdot 10^{-11}\text{s}$ , yielding one value for minimal (Barus-related) fragility  $\mu_p \approx 13$ , for arbitrary tested isotherm. All these led to a new definition of apparent fragility  $m_T^{\Delta P}$ , which can be linked to the ‘old’ one as follows [113]:

$$m_T^{\Delta P} = \frac{d \log_{10} \tau(P)}{d(\Delta P / \Delta P_g)} = \Delta P_g \frac{d \log_{10} \tau(P)}{d(\Delta P)} = \frac{\Delta P_g}{P_g} \frac{d \log_{10} \tau(P)}{d(P/P_g)} = \frac{\Delta P_g}{P_g} m_T(P) \tag{59}$$

where  $P = P - P_{SL}$ ,  $\Delta P_g = P_g - P_{SL}$  and  $P \leq P_g$ .

The new PVFT Eq. (58) contains four adjustable parameters. However, their validity can be tested by derivative-based analysis given below, which also yields optimal values of basic parameters [110]:

$$\left[ \frac{d \ln \tau(P)}{dP} \right]^{-1/2} = (D_P P_0)^{-1/2} P_0 - (D_P P)^{-1/2} P = A + BP \tag{60}$$

$$\left[ \frac{d \ln \tau(P)}{dP} \right]^{-1/2} = [D_P^{SL} (P_0 - P_{SL})]^{-1/2} P_0 - [D_P^{SL} (P_0 - P_{SL})]^{-1/2} P = A + BP \tag{61}$$

Eq. (60) is for basic PVFT and Eq. (55) and new N-PVFT Eq. (58). The comparison of Eqs. (60) and (61) show a link between fragility strength [110]:  $D_P^{SL} = D_P [(P_0 - P_{SL}) / P_0]$ .

Despite the PVFT relation's success, none theoretical model offers its derivation. Notwithstanding, one may transform the basic VFT Eq. (3) into the PVFT Eq. (53) by a simple substitution  $T = A/P$ :  $\tau(T) = \tau_{\infty}(T) \exp(D_T T_0 / (T - T_0)) \Rightarrow$ .

$\tau(P) = \tau_{\infty} \exp[D_T (A/P_0) / ((A/P) - (A/P_0))] = \tau_{\infty} \exp[D_T P / (P_0 - P)]$ . Such a simple link leads to a question of whether significant problems of the basic VFT relation also extend to PVFT one.

Notably, a relation resembling basic PVFT Eq. (55) was reported in 1963 by Roelands et al. (1963):  $\eta(P) = \eta_0 \exp(\alpha_0 P / (1 + R_3 P))$ , where  $R_3$  and  $\alpha_0$  are constants, for describing viscosity changes in lubricating oils [136]. One can also consider yet another relation, introduced by Roeland, originally for viscosity [136]:

$$\tau(P) = \tau_{\infty} \exp(R_1 P^{R_2}) \tag{62}$$

where  $R_1$  and  $R_2$  are system-dependent empirical constants.

Although heuristic considerations developed this relation in ref. [136], it can also be directly derived from the Avramov-Milchev (AM) model scaling relation. Namely, taking into account the basic relationship between cooling and compressing:

$$\tau(T) = \tau_{\infty} \exp\left(\frac{A_M}{T^D}\right) \Rightarrow T = \frac{A}{P} \Rightarrow \tau(P) = \tau_{\infty} \exp(A_M P^D) \tag{63}$$

It shows that  $R_2$  parameter in Roelands Eq. (62) reflects the pressure-related fragility. Note that Eqs. (62) and (63) suffer from the same problem with pre-exponential factor values like basic PVFT Eq. (55). This problem disappears if an 'extended version' of Eqs. (62) and (63) is considered:

$$\tau(P) = \tau_{\infty} \exp(R_1' (P - P_{SL})^{R_2'}) = \tau_{\infty} \exp(R_1' (\Delta P)^{R_2'}) \tag{64}$$

where the absolute stability limit pressure  $P_{SL} < 0$ .

The following distortions-sensitive test can be proposed:

$$\begin{aligned} \ln \tau(P) = \ln \tau_{\infty} + R_1' (\Delta P)^{R_2'} &\Rightarrow \frac{d \ln \tau(P)}{dP} = R_1' R_2' (\Delta P)^{R_2' - 1} \Rightarrow \\ \Rightarrow \ln \left( \frac{d \ln \tau(P)}{dP} \right) = \ln V^{\#}(P) &= R_1' R_2' (R_2' - 1) \ln(\Delta P) \end{aligned} \tag{65}$$

It can be simplified to the following dependence for the basic Roeland Eq. (62):

$$\ln \left( \frac{d \ln \tau(P)}{dP} \right) = \ln P \tag{66}$$

where  $R = R_1' R_2' (R_2' - 1)$ .

Eqs. (58) and (60) can be validated by the linear domain appears in the plot  $\ln V^{\#}(P)$  vs  $P$  or  $\Delta P$ . Subsequent linear regression fit may yield optimal values of basic parameters. The above reasoning can be implemented for introducing other relations describing pressure-related SB dynamics. Taking MYEGA Eq. (12) as a reference, one may propose its pressure counterpart:

$$\tau(T) = \tau_{\infty} \exp \left[ \frac{C}{T} \exp \left( \frac{K}{T} \right) \right] \Rightarrow T = \frac{A}{P} \Rightarrow \tau(P) = \tau_{\infty} \exp(C' P \exp(K' P)) \tag{67}$$

where,  $C' = C/A$  and  $K' = K/A$ . I.

It can be validated by the appearance of the linear domain in the plot defined by the following relation:

$$\ln \tau(P) = \ln \tau_{\infty} + C' P \exp(K' P) \Rightarrow V^{\#} = \frac{\ln \tau(P)}{dP} = C' \exp(K' P) [K' P + 1] \Rightarrow$$

$$\ln V^\# = \ln C' + K'P + \ln(K'P + 1) \approx 2K'P + \ln C' = aP + b \tag{68}$$

where the term  $\ln(K'P + 1)$  is expanded in the Taylor series.

We would like to name the pressure-related Eq. (67) as the ‘Unipress’ equation.<sup>2</sup>

The question arises for the advantage of Eq. (67) over PVFT or Roland relations. Notable that for the temperatures-related previtreous behavior the explicit prevalence of MYEGA relation over the VFT and AM descriptions was shown above. Fig. 12 shows the SB-type slowing down of the primary relaxation time in glycerol and xylitol in the enormous, GPa domain. High-pressure BDS studies are still limited to frequency range  $f < 10\text{MHz}$ , i.e., relaxation time  $\tau < 10^{-7}\text{s}$ . It means that only ultraviscous/ultraslow domain is directly available experimentally for glass forming systems via BDS. Fig. 13 presents the fairly validation of the Unipress Eq. (67), based on the distortions-sensitive analysis defined by Eq. (68). Note linear behavior, which can also support determining of optimal parameters values for Eq. (67) and the explicit manifestation of two dynamical domains.

Figs. 14 and 15 show distortions sensitive comparison of the PVFT (Eqs. (55) and the critical-like Eqs. (72), using data transformations defined by Eqs. (60) and (71), respectively. The analysis is based on experimental results given in Fig. 12. In both cases, the evident prevalence of the critical-like portrayal is manifested via explicit linear behavior. For the ‘standard’ PVFT description only an effective portrayal in a limited range of pressure can be considered.

One may also consider RFOT [85] glass transition model checkpoint relation toward its pressure counterpart:

$$\tau(T) = \tau_\infty \exp\left(\frac{A_G}{T(S_C(T))^\alpha}\right) \Rightarrow \tau(P) = \tau_\infty \exp(A_G P (S_C(P))^\alpha) \tag{69}$$

where basic AG model is related to the exponent  $\alpha = 1$ .

Following Eq. (69) one can propose the relation for pressure evolution of the configurational entropy:

$$S_C(P) = \frac{S_0}{(P_0 - P)^n} \tag{70}$$

where the exponent  $n$  may be related to both empirical symmetry-related exponent  $n$  and the RFOT exponent  $\alpha$ . For experimental validation of Eq. (66) necessary is challenging and still non-available pressure-related changes in configurational entropy.

The above discussion of Super-Barus dynamics has been tested using the Author’s experimental data for glycerol and xylitol. Such results are still hardly evidenced, particularly when considering GPa domain. The first challenging problem for studies under a high-pressure liquid system is isolating tested samples from a pressurized medium.

Recently, it has been discovered that transforming  $\tau(P)$  experimental data from the SB-type previtreous domain to pressure-related steepness index, i.e., apparent fragility ‘universal’ dependence for plot  $[m_T(P)]^{-1}$  vs, the simple and presumably universal evolution emerges [137]:

$$\frac{1}{m_T(P)} = a_{HP} + b_{HP}P \rightarrow m_T(P) = \frac{A_{HP}}{P^* - P} \tag{71}$$

where  $P_B^{1/m} < P < P_g$  and  $P^* > P_g$ ; singular pressure is estimated via the condition  $1/m_T(P_g^*) = 0$ .

Linking Eq. (71) with the definition of pressure-related apparent fragility, one obtains a differential equation, which solution leads to new critical-like relation for portraying pressure-related previtreous dynamics [137]:

$$\tau(P) = \tau_{\infty P} (P^* - P)^{-\Psi} \tag{72}$$

Using the preliminary analysis via Eq. (67) one may determine a singular pressure  $1/m_T(P^*) = 0$  or  $1/V^\#(P) = 0$  and then ‘discontinuity’:  $\Delta P_g^* = P_g^* - P_g$ . All these allow estimating the power exponent in Eq. 568:  $\Psi = \ln 10 \left( \frac{\Delta P_g^*}{P_g^*} \right) m_T(P_g)$ .

As mentioned in this section, estimating the evolution of apparent activation energy hypothetically responsible for previtreous slowing down requires the solution of a differential equation associated with the second-order derivative of experimental data. For the pressure path, the leading role plays Barus-Williams Eq. (46) governed by apparent activation volume. Most often, it is determined as  $V^\#(P) = d \ln \tau(P) / dP$ . However, such estimation for SB behavior is incorrect, namely based on SB Eq. (43) one obtains [138]:

$$V^\#(P) = \frac{d \ln \tau(P)}{dP} = \left( \frac{1}{RT} \right) V_a(P) + \left( \frac{1}{RT} \right) P \frac{dV_a(P)}{dP}, \text{ for } T = \text{const} \tag{73}$$

The above relation clearly shows that  $V^\#(P) \neq V_a(P)$ , except in the case  $P \rightarrow 0$  or for basic Barus behavior. As shown in ref. [138] for SB dynamics  $V^\#(P) \propto m_T(P)$ . However, for pressure-related previtreous effects, the pre-exponential factor is perfectly known what allows to calculate of the real apparent activation volume directly from the SB Eq. (43) [138]:

<sup>2</sup> Following the 50th years anniversary of IHPP PAS ‘Unipress’.

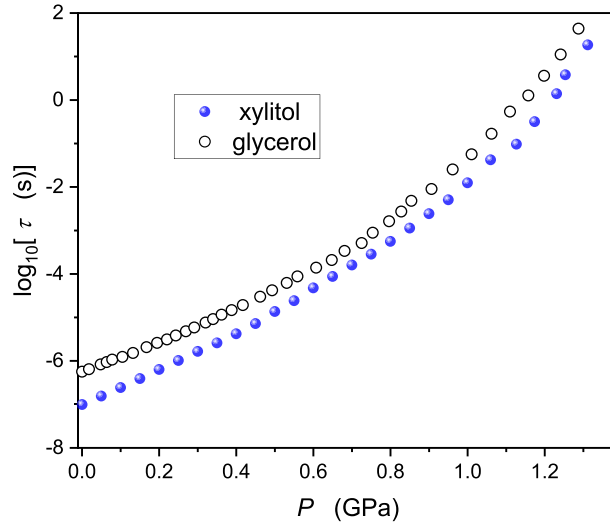


Fig. 12. Pressure evolution of primary relaxation time in super-pressed xylitol ( $T = 280$  K isotherm) and glycerol ( $T = 250$  K isotherm).

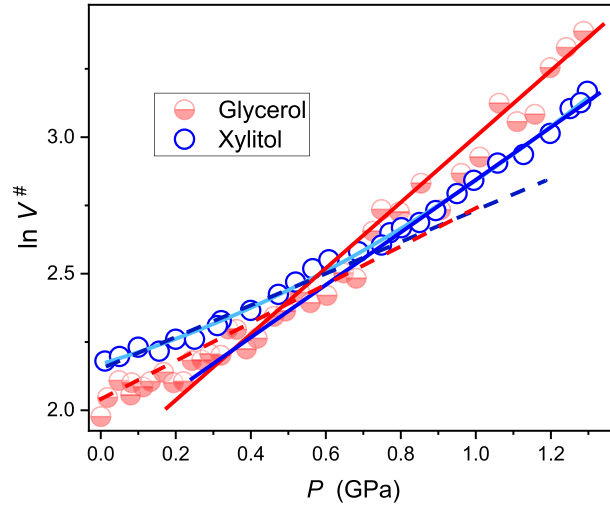


Fig. 13. Linearized and derivative-based analysis tested the validity of the portrayal of  $\tau(P)$  experimental data shown in Fig. 11, using the Unipress Eq. (63). Domains of its validity are indicated by the linear behavior (see Eq. (64)). Solid and dashed lines are for high pressures (non-ergodic, near  $P_g$ ) and low pressures (ergodic, remote from  $P_g$ ) dynamic domains.

$$V_a(P) = \frac{RT}{P} \ln\left(\frac{\tau(P)}{\tau_\infty}\right), \quad T = const \tag{74}$$

In ref. [121] also, the relation for pressure evolution of apparent activation volume was derived:

$$V_a(P) = \frac{C}{\Delta P} + \frac{\Psi}{\Delta P} \ln|P^* - P| \tag{75}$$

where  $C = const$  and  $\Delta P = |P - P_{SL}|$ ,  $P_{SL} < 0$  is for the absolute stability limit hidden in the negative pressures domain.

Notably, ‘traditional’ (but erroneous) dependence is qualitatively different [138]:

$$m_T(P) V^\#(P) \frac{1}{(P_g^* - P)^\Psi} \tag{76}$$

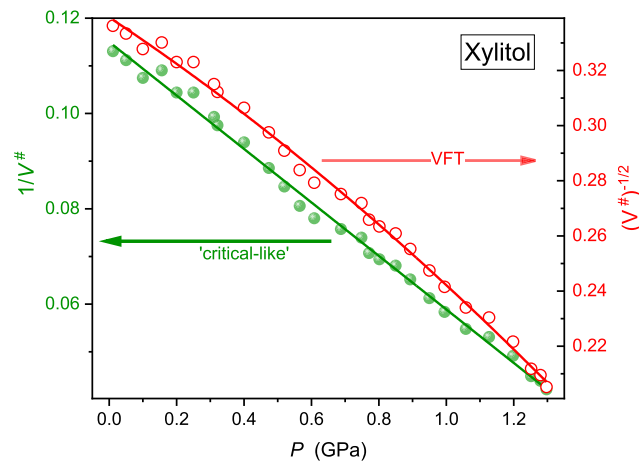


**Fig. 14.** Linearized and derivative-based focused testing for PVFT (Eqs. (55), 60) and critical-like portrayals (Eqs. (72), 71) in super-pressed xylitol, based on experimental data shown in Fig. 12. Mentioned scaling relations are validated by the linear behavior's emergence, which occurs only for the critical-like portrayal. Note:  $V^\#(P) = \text{dln}\tau(P)/\text{d}P$ .

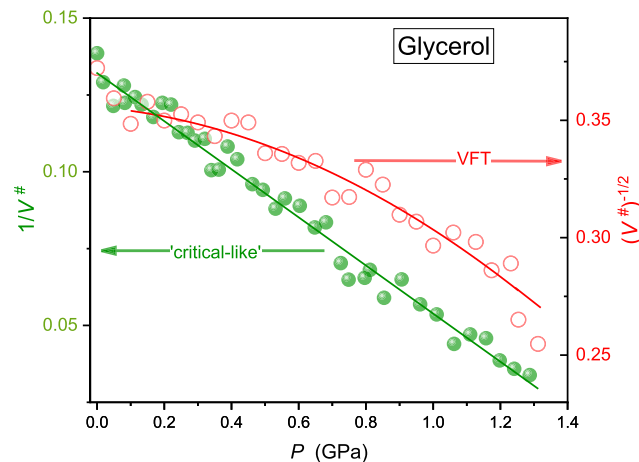


**Fig. 15.** Linearized and derivative-based focused on testing PVFT (Eqs. (55), 60) and critical-like portrayals (Eqs. (72), 71) in super-pressed glycerol, based on experimental data shown in Fig. 12. Scaling relations are validated by the emergence of linear behavior, which occurs only for the critical-like portrayal. Note:  $V^\#(P) = \text{dln}\tau(P)/\text{d}P$ .

## 7. The violation of Super-Barus previtreous behavior

The above discussion addressed Super-Arrhenius-type previtreous behavior on cooling and Super-Barus-type behavior on compressing. They are associated with an extreme and systematic previtreous rise of viscosity or slowing down for relaxation time. However, the experimental evolution of  $\eta(P)$  or  $\tau(P)$  may also exhibit a set of 'anomalous' patterns, namely:

- (i) Up to moderate pressures changes  $\eta(P)$  or  $\tau(P)$  may be weaker than Super-Barus, or even basic Barus behavior is observed. On further compressing, the return to SB pattern occurs. It is called the 'inflection' phenomenon. Such a behavior is often observed for elastohydrodynamic lubrication (EHL), which is important for machinery applications. [139–141].
- (ii)  $\eta(P)$  or  $\tau(P)$  may decrease during compressing. It can be preceded by almost constant changes or even a slight increase at low-moderate pressures. Such behavior is often observed in relevant geophysical systems [142,143].
- (iii) Evolution of  $\eta(P)$  or  $\tau(P)$  can change from 'fragile' SB behavior to a 'strong' one or almost Barus pattern when the temperature of the tested isotherm increases. It is named as the inflection phenomenon [144–149].

Finally, one raises the question, why  $\tau(T)$  or  $\eta(T)$  changes are described solely by 'strong' or 'fragile' SB behavior?

This section discusses the possible coherent picture linking the above patterns for viscosity and the coupled primary relaxation time. As indicated above, viscosity and primary relaxation time behavior are coupled via Debye-Stokes-Einstein relation [1. The technological importance of case (i) leads to heuristic relations that could portray such a behavior. The basic one was proposed in 1952

by McEwan, 1952 [141,144]:

$$\eta(P) = \eta_0 \exp\left(1 + \frac{P}{(q/a)}\right)^q \tag{77}$$

where  $\eta_0, a, q$  are constant parameters.

A few decades later, analysis that recalls Tait classical equation of state for pressure-related changes of volume/density led to dependence [141]:

$$\eta(P) = A \exp\left[B \ln\left(\frac{C+P}{C+P_r}\right)\right] \tag{78}$$

where  $P_r$  denotes the reference pressure. McEwan Eq. (77) may be retrieved from the above relation for  $P_r \approx 0$ .

The authors of this paper suggest that McEwan relation may also be derived by the use of the extended Avramov-Milchev Eq. (21), namely

$$\eta(T, P) = \tau_\infty \exp\left(\frac{A_M}{T}\right)^D = \eta_\infty \exp\left(\mu \ln 10 \left(\frac{T_g(P)}{T}\right)^D\right) \tag{79}$$

where  $\mu = \log_{10} \tau(T_g, P_g) - \log_{10} \tau_\infty$  is the minimal, reference fragility. The parallel of this relation can be written for viscosity.

Substituting the Andersson-Andersson (AA) relation [150] for pressure evolution of glass temperature  $T_g(P) = T_0(1 + P/a)^{1/b}$  one obtains a relation in agreement with Eq. (77):

$$\eta(P) = \eta_\infty \exp\left(\frac{\mu \ln 10}{T^D} \left(1 + \frac{P}{a}\right)^{D/b}\right) \propto C \left(1 + \frac{P}{a}\right)^{D/b} \tag{80}$$

Recalling analysis of AA relation, which is parallel to Simon-Glatzel dependence used for pressure evolution of melting temperature, the exponent  $b$  is related to the first derivative of bulk modulus and  $a$  to bulk modulus itself.

For describing  $\eta(P)$  or  $\tau(P)$  in a broad range of pressures, including the inflection phenomenon, i.e., crossover from McEwan to SB dynamics pattern, Paluch et al. [128,130] proposed heuristic link of McEwan Eq. (77) and PVFT Eq. (55):

$$\tau(P) = \tau_\infty \exp\left(1 + \frac{P}{(q/a)}\right)^q \exp\left(\frac{D_P P}{P_0 - P}\right) \tag{81}$$

It was applied successfully for portraying pressure changes of relaxation time, viscosity, or electric conductivity upon compressing. Bair proposed to supplement it with the Casalini-Roland (C-R) pressure counterpart by Stickel et al. analysis [147],  $\varphi_p(P) = [d \log_{10} \eta(P) / dP]^{-1/2}$  or  $\varphi_p(P) = [d \log_{10} \tau(P) / dP]^{-1/2}$  to validate PVFT behavior at higher pressures. However, such an analysis assumes a priori universality of VFT and PVFT pre-vitreous behavior, which seems to be questionable, as discussed above. A significant problem of the ‘hybrid’ Eq. (81) constitutes 5 adjustable parameters, leading to a considerable error of parameters in the non-linear fitting as well as to ‘fitting flexibility’ able to offer a parameterization in a broad range of parameters.

One can propose alternative ‘hybrid’ relations, which can be supported by convenient preliminary derivative-based analysis, reducing the number of adjustable parameters, namely:

$$\eta(P) = \eta_0 \left(1 + \frac{P}{a_l}\right)^{q_l} \left(1 + \frac{P}{a_h}\right)^{q_h} \tag{82}$$

where indices ‘ $l$ ’ and ‘ $h$ ’ stand for the low and high-pressure domains (below and above the inflection), power exponents  $q_l > 0$  and  $q_h < 0$ .

Alternatively, one can consider the ‘double-critical-like’ hybrid relation:

$$\eta(P) = \eta_0 |P_l^* - P|^{q_l} |P_h^* - P|^{q_h} \tag{83}$$

where power exponents  $q_l > 0$  and  $q_h < 0$  and  $P^*$  denote the extrapolated singular pressure.

Let’s consider linearized derivative-based and distortions-sensitive analysis for leading terms for the above dependencies. For the leading term in critical-type Eq. (83):

$$\log_{10} \eta(P) = \log_{10} \eta_0 + \varphi \log_{10} |P^* - P| \Rightarrow \frac{d \log_{10} \eta(P)}{dP} = \frac{\varphi}{\ln 10} \frac{1}{|P - P^*|} \Rightarrow \left[\frac{d \log_{10} \eta(P)}{dP}\right]^{-1} = \frac{\ln 10}{\varphi} |P - P^*| = AP - B \tag{84}$$

and then  $\varphi = \ln 10 / A \approx 2.3 / A$ , and  $P^* = B / A$ .

For the leading term in McEwan-type Eq. (82):

$$\log_{10} \eta(P) = \log_{10} \eta_0 + q \log_{10} \left(1 + \frac{P}{a}\right) \Rightarrow \frac{d \log_{10} \eta(P)}{dP} = \frac{q}{\ln 10} \frac{1}{(a+P)/a} \Rightarrow \left[\frac{d \log_{10} \eta(P)}{dP}\right]^{-1} = \frac{\ln 10}{qa} (a+P) = AP + B \tag{85}$$

and then  $q = \ln 10/A \approx 2.3/A$  and  $a = B/A$ .

Hence, the same plot  $[d\log_{10}\eta(P)/dP]^{-1}$  vs  $P$  can verify a double-critical-type and double-McEwan-type relations by the emergence of a linear domain. Linear regression fit can yield optimal values of parameters:  $\varphi = q = \ln 10/A \approx 2.3/A$  and  $a = P^* = B/A$ . Remarkably, the latter is worth stressing since it is related to  $[d\log_{10}\eta(P)/dP]^{-1} = 0$ , easily determined graphically. Results of the analysis based on Eqs. (84) and (85) is shown in Fig. 17, for compressed di-isobutyl phthalate. The plot shows that the described analysis enables the precise determination of the inflection pressure for the given tested isotherm. Values of related parameters determined via the linear regression fit are also given in the figure. Results presented in Fig. 17 have been obtained using experimental data presented in Fig. 16. The central part of the plot shows the fair portrayal of  $\eta(P)$  experimental data by single critical-type (Eq. (82)) and McEwan-type (Eq.(83)) terms, separately for both domains, below and above  $P_{inf.}$ , with parameters given in Fig. 17 for each domain. The visible overlapping of both types of portrayals for  $P < P_{inf.}$  shows that the basic McEwan relation is equivalent/isomorphic to a critical-like one, with the exponent  $\varphi > 0$  and singular pressure  $P^* < 0$ . For both cases, extension into the negative pressure domain, down  $P = P^* = a$  is possible.

The common description of both domains (for pressures below and above the inflection) by ‘double relations, Eq. (82) or (83), yields a fair portrayal of experimental data, as shown in the inset in Fig. 16. However, a comparable fitting quality can be obtained for parameters different even by 50 % or more, particularly regarding the power exponent  $q$  or  $\varphi$ . Results presented in the inset in Fig. 15 are for singular pressure values ( $P^*$ ,  $a$ ). As indicated below, the inflection phenomenon may be considered as the propagation of an impact of a maximum of  $T_g(P)$  curve, for tested isotherms located above the maximum. Generally, at least in liquids, one may expect vitrification to be associated with ‘mechanism I’ and ‘mechanism II’ [127]. The latter emerges under extreme pressures and is related to the domination of repulsive, hard-sphere-type interactions. For lower pressures, an interplay between attractive and repulsive interaction may even lead to a crossover in compressing. This may give the emergence of  $T_g(P)$  maximum and following portrayal [82,151,152]:

$$T_g(P) = F(P)D(P) = T_g^0 \left(1 + \frac{\Delta P}{\Pi}\right)^{1/b} \exp\left(\frac{P}{c}\right) = T_g^0 \left(1 + \frac{P - P_g^0}{\pi + P_g^0}\right)^{1/b} \exp\left(\frac{P}{c}\right) \tag{86}$$

where  $F(P)$  and  $D(P)$  are for the rising (SG-type) and damping terms,  $\pi < 0$  is for the terminal of absolute stability limit pressure at  $T = 0$ , and  $c$  is for the damping pressure coefficient. The above relation is valid for an arbitrary pressure along  $T_g(P)$  curve and may penetrate the negative pressure domain. It can even describe systems where the maximum is hidden in the negative pressures domain. It parallel obeys for pressure dependence of melting temperature  $T_m(P)$ . Worth recalling is a link between both magnitudes, known as the Turnbull criterion:  $T_m/T_g \approx w < 1$ . For systems particularly ‘easily’ passing  $T_m$  and entering the supercooled, pre-vitreous domain  $w \approx 2/3$  is suggested. Assuming  $T_g^0 = T_g(P = 0.1MPa)$  and  $P_g^0 = 0.1MPa$  one may approximate the above relation in the form first derived by Rein and Demus [153] and recalled by Kechin [154]:

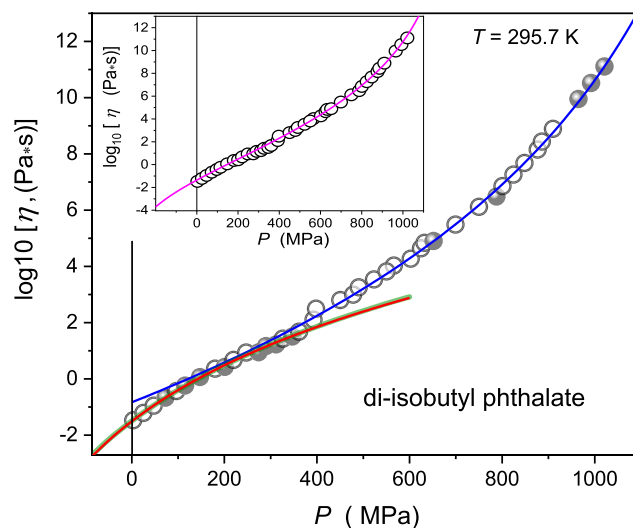


**Fig. 16.** Pressure dependence of viscosity in di-isobutyl phthalate (DIIB) for the isotherm  $T = 320$  K. Open circles are related to viscosity measurement [156, 157] supplemented by scaled primary dielectric relaxation time. Full circles are for the authors scaled primary relaxation time measurement, supplementing mentioned results. Blue, green, and red curves are related to Eqs. (84) with parameters derived separately for each domain, as shown in Fig. 17. The inset shows the double-critical portrayal parameterization via Eq. (84).

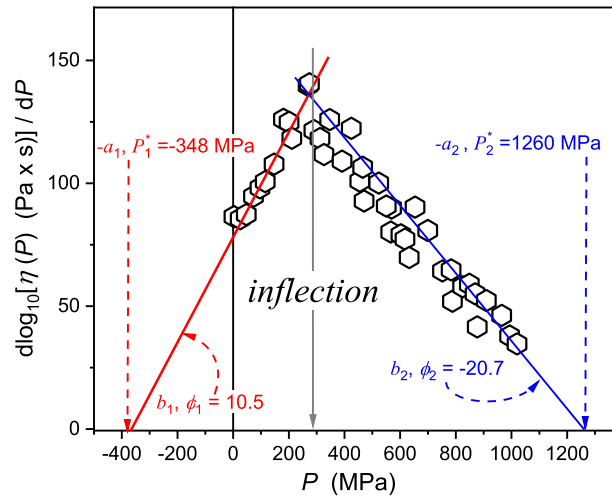


**Fig. 17.** Inflection showed based on results of derivative-based analysis related to Eqs. (79) and (80) obtained in di-isobutyl phthalate taken from Fig. 15.

$$T_g(P) \approx T_g^0 \left(1 + \frac{P}{\pi}\right)^{1/b} \exp\left(\frac{P}{c}\right) \tag{87}$$

It obeys for  $P \geq 0$ . When neglecting a damping term ( $c \rightarrow \infty$ ) it has a form of the Andersson-Andersson (AA) equation [150] or glass temperatures or the Simon-Glatzel relation for melting temperature [127]. For such an approximation  $T_g(P)$  and  $T_m(P)$  permanently increase when compressing. Notwithstanding, AA- or SG-related approximations may be used below the hypothetical maximum of  $T_g(P)$  or  $T_m(P)$ , for systems where  $dT_{g,m}(P)/dP > 0$ .

In a hybrid Eq. (78) and ‘doubled’ Eqs. (79) and (80) a low-pressure behavior for  $P < P_{inf}$  is associated with basic McEwan Eq. (73). Following the derivation of Eq. (75), its pressure characterization is determined by  $T_g(P)$  behavior, i.e., assuming the AA relation as a background and omitting decreases of  $T_g(P)$  passing the maximum ( $dT_g/dP < 0$ ). The latter means that the influence of vitrification ‘mechanism I’ diminish for  $> P_{inf}$ . However, for the basic McEwan equation impact of ‘mechanism I’ continuously increases when passing  $P_{inf}$ , leading to the parasitic bias of fitting results. Consequently, new ‘doubled’ Eqs. (79, 80) as well as the popular ‘hybrid one’ (Eq. (78)) may be considered only as an effective, practical tool for portrayal  $\eta(P)$ ,  $\tau(P)$  or  $\sigma(P)$  dependences exhibiting the inflection phenomenon. Consequently, fundamentally justified seems to be the separate treatment of domain  $P < P_{inf}$  as single McEwan-type dependence and for  $P > P_{inf}$  by PVFT or critical-like relations with the exponent  $\varphi_h < 0$ . Leading parameters can be supported by the derivative-based estimations shown in Fig. 16. However, it is possible to propose a new ‘hybrid’ relation describing the whole range of pressures and coupled to reference values of parameters given by validation preliminary derivative-based analysis (Fig. 15). It can be ‘designed’ linking Eqs. (79) and (86). It allows proposing the McEwan-type equation, which impact diminishes when passing  $P_{inf}$ .

$$\begin{aligned} \eta(P) &= \eta_\infty \exp\left(\frac{\mu \ln 10}{T^D} \left(1 + \frac{P}{a}\right)^{D/b} \exp\left(\frac{P}{c/D}\right)\right) \propto C \left(1 + \frac{P}{a}\right)^{D/b} \exp\left(\frac{P}{c/D}\right) \Rightarrow \\ \Rightarrow \eta(P) &= \eta_0 \left(1 + \frac{P}{a}\right)^b \exp\left(\frac{P}{c}\right) \end{aligned} \tag{88}$$

where  $P_{inf} > P \geq 0$ , extension into negative pressures domain requires substitution  $P \rightarrow \Delta P = P - P_{SL}$ . The latter can be estimated as  $P_{SL} a = \pi$ .

To describe the whole range of pressures above and below  $P_{inf}$ , the following hybrid relation can be considered:

$$\eta(P) = \eta_0 \left(1 + \frac{P}{a}\right)^b \exp\left(\frac{P}{c}\right) (P_{II}^* - P)^{\varphi_h} \tag{89}$$

for  $P > 0$ .

Taking into account the above considerations, an extension into the following extension may also cover the negative pressures domain:

$$\eta(P) = \eta_0 \left(1 + \frac{P+a}{a}\right)^b \exp\left(\frac{P+a}{c}\right) (P_{II}^* - P)^{\varphi_h} \tag{90}$$

Eqs. (86) and (87) contain 5 adjustable parameters. For comparison, the hybrid Eq. (78) by Paluch et al. also includes 5 parameters.

However, in Eqs. (86) and (87) four parameters ( $a, b'$ ) and ( $P_{II}^*, \varphi_h$ ) can be determined from the preliminary derivative-based analysis shown in Fig. 16. The pre-exponential factor  $\eta_0 = \eta(P=0) \approx \eta(P=0.1\text{MPa})$ , i.e., it may be determined directly from the experiment. Consequently, for the final fitting, only the coefficient  $c$  (1 parameter) remains. Results of such portrayal are also shown in Fig. 16.

Fig. 18 schematically shows pressure evolution of glass temperature for a ‘model-liquid’. It contains both vitrification mechanisms (I, II) discussed above. The plot indicates the basic paths used for  $\eta(P)$  or  $\tau(P)$  studies. Path (1) is for ‘basic’ Super-Barus dynamics. For path (3) one expects the appearance of the inflection phenomenon when passing a dotted line related to  $P_{inf.}$ . This is a specific manifestation of the propagation of a maximum of  $T_g(P)$  curve impact in the over-glass domain of supercooled glass-forming liquid. The ‘inflection area’ is terminated by paths (4) and (2). For the latter, near the top of  $T_g(P)$  curve can cause significant or even negligible changes in dynamics. When passing the maximum, for  $P > P_{inf.}$  one can expect even a slight decrease of  $\eta(P)$  or  $\tau(P)$  changes until the rise on further compressing, caused by approaching the ‘mechanism II’ glass transition line. The possibility of the emergence of such ‘S-shape’ behavior was recently indicated for compressed acetone. For path 4, the impact of the ‘inflection line’ diminishes, and one can expect strong dynamics, close to basic Barus behavior until approaching the ‘mechanism II’ vitrification domain at extreme pressure. The gradual transformation from the ‘fragile’ to ‘strong’  $\eta(P)$  or  $\tau(P)$  evolution when increasing temperatures of tested isotherms can be found for glycerol, for instance. For paths (5) and (6) one can expect that  $\eta(P)$  or  $\tau(P)$  firstly increase on compressing until the rise associated with approaching the line related to the second vitrification mechanism emerges. For path (6) one can expect that, at first, the ‘flat’ domain associated with the proximity of  $T_g(P)$  curve maxim before the drop of  $\eta(P)$  associated with moving away from the ‘mechanism I’ glass transition curve starts to dominate. For some systems, the maximum of the  $T_g(P)$  can be hidden under negative pressures, and for such systems, the behavior associated with  $dT_g/dP < 0$  domain can be expected for pressures  $P > 0$  (paths 5 and 6). It can explain ‘anomalous’ patterns of viscosity changes observed in geophysical significant, strongly bonded, magmatic fluids [142,143]. Note that none of the above ‘anomalous’ patterns for  $\eta(P)$  or  $\tau(P)$  evolutions cannot occur for previtreous  $\eta(T)$  or  $\tau(T)$  changes, as explicitly shown in the results presented in Fig. 17. An exception can be expected for cooling under extreme pressures, close to the slowly approaching ‘mechanism II’ vitrification curve. However, no such experimental results are available yet.

## 8. Conclusions

The transition from the ‘liquid-like’ ultraviscous/ultraslow system to the solid glass state remains the grand challenge of solid-state physics and material engineering. The key cognitive attractor constitutes long-range previtreous changes of the primary ( $\alpha$ , structural) relaxation time or viscosity. Their portrayal is the essential checkpoint for theoretical models explaining the glass transition phenomenon. For decades the Vogel-Fulcher-Tammann (VFT), or alternatively Williams-Landel-Ferry (WLF), relations were considered as the symbolic presentation of the previtreous dynamics universality. Consequently, its derivation was used as the significant argument validating theoretical models: Adam-Gibbs entropic model, the basic free volume approach, or Tanaka’s critical model can serve as examples. However, the state-of-the-art tests explicitly showed that VFT portrayals can be considered only as an effective way of parameterization, for the vast majority of glass-forming systems. It was a significant motivation for developing glass transition models proposing different scaling relations for the previtreous dynamics. Two ways of experimental model-validation were used. The first one was related to showing the prevalence of the fitting quality against experimental data compared to other popular scaling relations.

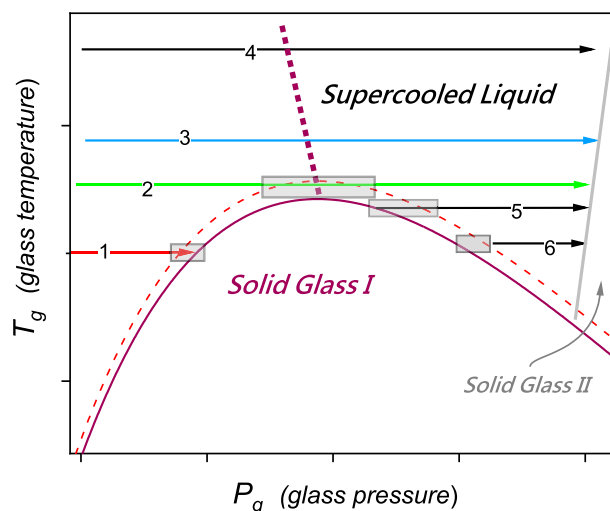


**Fig. 18.** Schematic plot of pressure evolution of glass temperature. The glass temperature is represented by  $\tau(P_g) = 100\text{s}$  and  $\eta(P_g) = 10^{13}\text{Poise}$  and the brown curve. Red dashed one indicates an isochronal/isoviscous curve slightly above glass transition  $\tau(P) = 10\text{s}$  and  $\eta(P) = 10^{12}\text{Poise}$ . Horizontal colored lines (1–4) indicate paths along which viscosity or relaxation time changes may be tested. The dotted vertical line indicates the suggested ‘inflection line’ above a maximum of  $T_g(P)$  curve. Squares in grey indicate different impacts of pressure changes near glass transition for selected paths.

Unfortunately, such an approach has not yielded conclusive results, particularly when a broader set of glass formers was taken into account. The second approach was related to the superposition of  $\tau(T)$  or  $\eta(T)$  experimental data for dozens of glass-formers in the plot with a scaled axis, according to the tested model-equation requirements. Data-scaling parameters are determined individually for each system, in prior. Hence, it is a 'tautological validation', with success guaranteed in advance.

As discussed in the given report, the problem may arise from omitting the fact that the previtreous domain extends well above the singular temperature ( $T^* = T_0, T_C$ ), i.e., for  $T > T_g = T^* + \Delta T^*$ , where the discontinuity  $\Delta T^* = T_g - T^* = 20 - 100$  K. Only the 'tail' of the previtreous effect is available for the empirical analysis. The region of strong, characteristic changes near  $T^*$  is inherently unavailable. Experiences from studies of weakly-discontinuous phase transitions show that even a small discontinuity  $\Delta T^* \sim 1$  K, can introduce crucial uncertainty to pretransitional effects.

Therefore, a methodology sensitive to subtle deviations of experimental data from the trend defined by a given scaling equation should be applied, such as the linearized derivative-based analysis, discussed in detail in the given report. It is associated with following steps:

(i) The transformation of experimental data to the apparent fragility, apparent enthalpy, or other alternative derivative representations:  $\tau(T) \Rightarrow m_P(T), H_a(T), d \ln \tau(T) / d(1/T)$

$$\text{or } \tau(P) \Rightarrow m_T(P), V^\#(P) = d \ln \tau(P) / dP.$$

(ii) Subsequently, relation showing  $m_P(T), H_a(T), \dots V^\#(P)$  changes are derived for selected scaling model-equations. Next, they are transformed into a linearized form.

(iii) The latter defines the way in which transformed experimental data should be presented. The appearance of a linear behavior validates the application of the selected scaling equation in the given temperature domain. Linear regression can yield optimal values of relevant parameters.

This report shows the implementation of the above protocol for the set of scaling equations validating a set of glass transition models. Notable that it is extended for the pressure path of approaching the glass transition, still poorly represented in the glass transition model analysis.

Following the discussion in this report only two types of model-equations seem to pass the distortions-sensitive tests, namely:

1. MYEGA Eq. (12) and its pressure counterpart: *Unipress* Eq. (67) - derived in the given report
2. Fragility-anomaly-related scaling equations: 'activation-critical' Eq. (33) for the temperature path and the 'critical' Eq. (72).

Notable that the SA-type previtreous slowing down or viscosity rise occurs on cooling for an arbitrary glass forming system. For compressing, the SB-type previtreous slowing down or viscosity rise also often takes place, but additionally, two 'anomalous' patterns also occurs: (i) 'speeding up' for  $\tau(P)$  or viscosity decrease on compressing, (ii) inflection-type changes on compressing.

This report shows that existing evidence enables the coherent explanation of all the above evolutions for temperature and pressure paths. For the latter, the way of the precise estimation of the inflection pressure matched with the new scaling relation for  $\tau(P)$  or  $\eta(P)$  portrayals is given.

The authors want to stress some other consequences of the resume presented in this report. In 1996 Stickel et al. [93] indicated the existence of two dynamical domains in the previtreous domain via the analysis of experimental data transformed using the 'Skickel operator'  $\varphi_T(T) = [d \log_{10} \tau(T) / d(1/T)]^{-1/2}$ , mainly used for determining the dynamic crossover temperature  $T_B$ . The pressure parallel based on experimental data transformed via the function:  $\varphi_P(P) = [d \log_{10} \tau(P) / dP]^{-1/2}$  for determining the crossover pressure  $P_B$  also was introduced [155]. However,  $\varphi_T(T)$  and  $\varphi_P(P)$  are directly coupled to VFT and PVFT relations. The general validity of VFT and PVFT equation is limited, as discussed in the given report. Hence, conclusions of numerous research reports [17–19, 107, 138, and ref. therein] exploring  $\varphi_T(T)$  and  $\varphi_P(P)$  for getting insight into the dynamical crossover should be re-considered.

The major part of the report is focused on the linearized distortions-sensitive and derivative-based analysis of  $\tau(T)$  experimental data to reveal 'hidden' features of the previtreous dynamics, particularly regarding possibilities of their portrayal by glass transition models related scaling equations. However, this report presents yet another innovative approach developed in the last decade based on the activation energy index. Worth stressing is the extension of this approach beyond the existing evidence, for CGE [66] and Roessler et al. [89] scaling equations. The report also addresses the related evolution of the configurational entropy changes developed in refs. [45,123]. This issue is worth stressing due to the emerging link to critical phenomena and local symmetry of the vitrifying system.

Just recently, the authors' noted one more issue requiring the reliable and validated extrapolation of the primary relaxation time well beyond the experimental liquid-like domain. Recently, it was discovered that annealing under moderate pressures,  $P \sim 1$  GPa, in the solid glass phase just below  $T_g$  can yield extraordinary properties, preserved after decompressing. Some of them are significant for innovative applications. One can recall exceptional surface hardness and densification in Gorilla-type glasses for innovative display covers [155] or 2–3 decades boost of electric conductivity in solid glasses, considered as cathodes in new generation batteries [156]. Notable, that generally compressing of crystalline or amorphous (well below  $T_g$ ) solids also can yield extraordinary material features. However, it requires tens – hundreds of GPa, and unique properties disappear after decompressing.

No explanation of unique features emerging due to annealing under 'moderate range' compressing in the shade of  $T_g$  has been proposed so far. The authors want to indicate, that very recently, Song et al. [157] announced the discovery of a new relaxation process in the previtreous domain, called the Slow Arrhenius process (SAP) to indicate its main features (i) the location in the low frequencies domain of  $\epsilon''(f)$  spectrum, well below the primary relaxation, (ii) the simple Arrhenius evolution of the related relaxation time  $\tau_{SAP}$ . It

was suggested in ref. [157] that, it can be significant for the overall equilibration rate coefficient, defined as:

$$\frac{1}{t_{eq.}} = \frac{c_{sap}}{\tau_{SAP}} + \frac{c_{\alpha}}{\tau_{\alpha}} \quad (91)$$

where  $c_{SAP}$ ,  $c_{\alpha}$  are constant coefficients, and  $\tau_{\alpha} = \tau$ .

Notable that SAP and the alpha relaxation process can smoothly extend into the solid glass. It is relatively easy detectable for  $\tau_{SAP}$  which changes are relatively mild, since they follow the basic changes Arrhenius pattern. The primary ( $\alpha$ ) relaxation time evolution terminates at  $T \approx T_g$ , where it reaches  $\tau(T_g) \approx 100$ s or alternatively  $\eta(T_g) \approx 10^{13}$ Poise. Below  $T_g$ , in the solid glass, the relaxation time boosts so strongly that its estimations of are impossible or at least extremely difficult.

For the solid glass state, Eq. (91) can mean that the solid glass below  $T_g$  can be split into the 'soft glass', near  $T_g$ , and the 'hard glass', well below  $T_g$ . The singularity associated with the evolution of  $\tau(T)$  can estimate the border between these domains. Consequently, extraordinary properties associated with annealing under moderate pressures and preserved after decompressing can be yielded in the 'soft glass domain', depending on the distance from  $T_g$ .

Although speculative and requiring focused studies, the latter section can indicate the existence of specific previtreous effects in the solid phase, below  $T_g$ , and the practical significance of a reliable and fundamentally justified description of the primary relaxation time evolution.

### CRediT authorship contribution statement

**Aleksandra Drozd-Rzoska:** Conceptualisation, Writing – original draft, Supervision. **Sylwester J. Rzoska:** Conceptualisation, Writing – original draft, Investigation, Formal analysis, Visualisation, Writing – review & editing. **Szymon Starzonek:** Conceptualisation, Writing – original draft, Investigation, Formal analysis, Visualisation, Writing – review & editing.

### Declaration of Competing Interest

The authors declare that they have no known competing financial interests or personal relationships that could have appeared to influence the work reported in this paper.

### Acknowledgments

Studies were carried out due to the National Centre for Science (NCN OPUS grant, Poland), ref. UMO-2017/25/B/ST3/02458, headed by Sylwester J. Rzoska, and ref. 2016/21/B/ST3/02203, headed by Aleksandra Drozd-Rzoska. Szymon Starzonek's work was supported by NCN Grant no. 2019/32/T/ST3/00621.

### References

- [1] Heyland A, Moroz LI. Signaling mechanisms underlying metamorphic transitions in animals. *Integr Comp Biol* 2006;46:743–59.
- [2] Klok CJ. Biological glass: a strategy to survive desiccation and heat. *J Exp Biol* 2010;213:4–10.
- [3] Roskosz M, Gillot J, Capet F, Roussel P, Leroux H. A sharp change in the mineralogy of annealed protoplanetary dust at the glass transition temperature. *A&A* 2011;529:A111.
- [4] Wadsworth FB, Heap AJ, Damby DE, Hess K-U, Najorka J, Vasseur J, et al. Dingwell Local geology controlled the feasibility of vitrifying Iron Age buildings. *Sci Rep* 2017;7:40028.
- [5] Pagacz J, Stach P, Natkaniac-Nowak L, Naglik B, Drzewicz Ap. Preliminary thermal characterization of natural resins from different botanical sources and geological environments. *J Therm Anal Calorim* 2019;138:4279–88.
- [6] Petters M, Kasparoglu S. Predicting the influence of particle size on the glass transition temperature and viscosity of secondary organic material. *Sci Rep* 2020;10:15170.
- [7] Roos YH. Glass transition temperature and its relevance in food processing. *Ann Rev Food Sci Technol* 2010;1:469–95.
- [8] Yadav NR, Gaikwad VL, Nair K, Kadam HM. Glass transition temperature: Basics and application in pharmaceutical sector. *Asian J Pharm* 2009;2:82–9.
- [9] Sahu S, Saraf S. Bioengineering techniques for the efficacy of herbal cosmetics Res. *J Topical and Cosmetic Sci* 2010;1:1–12.
- [10] Hoang Nguyen HT, Qi P, Rostagno M, Feteha A, Miller SA. The quest for high glass transition temperature bioplastics. *J Mater Chem A* 2018;6:9298–331.
- [11] Januchta K, Youngman RE, Goel A, Bauchy M, Logunov SL, Rzoska SJ, et al. Smedskjaer Discovery of ultra-crack-resistant oxide glasses with adaptive networks. *ACS Chem Mat* 2017;29:5865–76.
- [12] Baranowski P, Starzonek S, Drozd-Rzoska A, Rzoska SJ, Boćkowski M, Koblinski P, et al. Garbarczyk Multifold pressure-induced increase of electric conductivity in  $\text{LiFe}_{0.75}\text{V}_{0.10}\text{PO}_4$  glass. *Sci Rep* 2019;9:16607.
- [13] Zhao D, Wang M, Xiao G, Zou B. Thinking about the development of high-pressure experimental chemistry. *J Phys Chem Lett* 2020;11:7297–306.
- [14] Pegg DE. Principles of cryopreservation. *Methods Mol Biol* 2007;368:39–57.
- [15] Kennedy D, Norman C. What don't we know. Science's 125 Open Questions. In: 125<sup>th</sup> anniversary Science 1<sup>st</sup> July special issue; 2005.
- [16] Berthier L, Ediger M. Facets of the glass transition. *Phys Today* 2016;69:40–4.
- [17] Kremer F, Loidl A. Scaling of Relaxation Processes. Berlin: Springer; 2018.
- [18] Ramirez R. An Introduction to Glass Transition. London: Nova Sci Pub; 2019.
- [19] McKenna GB. Glass transition: challenges of extreme time scales and other interesting problems. *Rubber Chem and Technol* 2020;93:79–120.
- [20] Anisimov Ma. Critical Phenomena in Liquids and Liquid Crystals. Reading: Gordon and Breach; 1992.
- [21] Honig J, Spalek J. A Primer to the Theory of Critical Phenomena. Amsterdam: Elsevier; 2018.
- [22] Chrapeć J, Rzoska SJ, Ziolo J. Pseudospinodal curve for binary solutions determined from the nonlinear dielectric effect. *Chem Phys* 1987;111:155–60.
- [23] Rzoska SJ, Drozd-Rzoska A, Mukherjee PK, Lopez DO, Martinez Gracia JC. Distortion-sensitive insight into the pretransitional behavior of 4-n-octyloxy-4'-cyanobiphenyl (8OCB). *J Phys: Condens Matt* 2013;25:245105.
- [24] Drozd-Rzoska A, Rzoska S, Pawlus S, Ziolo J. Complex dynamics of supercooling n-butylcyanobiphenyl (4CB). *Phys Rev E* 2005;72:031501.

- [25] Drozd-Rzoska A, Rzoska SJ, Ziolo J. Mean-field behaviour of the low frequency non-linear dielectric effect in the isotropic phase of nematic and smectic n-alkylcyanobiphenyls. *Liquid Crystals* 1996;21:273–7.
- [26] Drozd-Rzoska A, Rzoska SJ, Czupryński K. Phase transitions from the isotropic liquid to liquid crystalline mesophases studied by “linear” and “nonlinear” static dielectric permittivity. *Phys Rev E* 2000;61:5355–60.
- [27] Drozd-Rzoska A, Starzonek S, Rzoska SJ, Łoś J, Kutnyak Z, Kralj Zs. Pretransitional Effects of the Isotropic Liquid-Plastic Crystal Transition. *Molecules* 2021;26:429.
- [28] Drozd-Rzoska A, Rzoska SJ, Szpakiewicz-Szatan A, Starzonek S, Łoś J, Orzechowski K. Supercritical anomalies in liquid ODIC-forming cyclooctanol under the strong electric field. *J Mol Liq* 2022;345:1178491.
- [29] Drozd-Rzoska A, Rzoska SJ, Szpakiewicz-Szatan A, Łoś J, Orzechowski K. Pretransitional and premelting effects in menthol. *Chem Phys Lett* 2022;793:139461.
- [30] Suzuki A, Masuko M, Wakisaka K. Pressure-dependence of dielectric relaxation time in poly(propylene glycol) and its application to high-pressure viscosity estimation. *Tribol Int* 2002;35:55–63.
- [31] Starzonek S, Rzoska SJ, Drozd-Rzoska A, Pawlus S, Martinez-Garcia JC, Kistersky L. Fractional Debye–Stokes–Einstein behaviour in an ultraviscous nanocolloid: glycerol and silver nanoparticles. *Soft Matter* 2011;5:5554–62.
- [32] Angell CA. Strong and fragile liquids. In: Ngai KL, Wright GB, editors. *Relaxations in Complex Systems*. Washington DC: NRL; 1985. p. 13–42.
- [33] Angell CA. Structural instability and relaxation in liquid and glassy phases near the fragile liquid limit. *J Non-Cryst Solids* 1988;102:205–21.
- [34] Böhmer R, Ngai KL, Angell CA, Plazek DJ. Nonexponential relaxations in strong and fragile glass formers. *J Chem Phys* 1993;99:4201–9.
- [35] Angell CA. Formation of glasses from liquids and biopolymers. *Science* 1995;267:1924–35.
- [36] Mauro JC, Loucks RJ. Impact of fragility on enthalpy relaxation in glass. *Phys Rev E* 2008;78:021502.
- [37] Wang L-M, Mauro J. An upper limit to kinetic fragility in glass-forming liquids. *J Chem Phys* 2011;134:044522.
- [38] Martinez Garcia JC, Tamarit JL, Rzoska SJ. Enthalpy space analysis of the evolution of the primary relaxation time in ultraslowing systems. *J Chem Phys* 2011;134:024512.
- [39] Vogel H. Temperaturabhängigkeitsgesetz der viskosität von flüssigkeiten. *Phys Zeit* 1921;22:645–6.
- [40] Fulcher GS. Analysis of recent measurements of the viscosity of glasses. *J Am Ceram Soc* 1925;8. pp. 339-335.
- [41] Tammann G. Glasses as supercooled liquids. *J Soc Glass Technol* 1925;9:166–85.
- [42] Ngai KL. Relaxation and Diffusion in Complex Systems. Berlin: Springer; 2010.
- [43] Ojovan MI. On viscous flow in glass-forming organic liquids. *Molecules* 2020;25:4029.
- [44] Roggero A, Causse N, Pebere N, Dantras E. VFT to Arrhenius crossover at the dynamic glass transition of an epoxy network as revealed by dielectric experiments in continuous immersion. *Polymer* 2022;241:124542.
- [45] Williams ML, Landel RF, Ferry JD. The temperature dependence of relaxation mechanisms in amorphous polymers and other glass-forming liquids. *J Am Chem Soc* 1955;77:3701–6.
- [46] Wang L, Angell CA, Richert R. Fragility and thermodynamics in nonpolymeric glass-forming liquids. *J Chem Phys* 2006;125:074505.
- [47] Senkov ON, Miracle DB. Correlation between thermodynamic and kinetic fragilities in nonpolymeric glass-forming liquids. *J Chem Phys* 2008;128:124508.
- [48] Lee C-S, Lulli M, Zhang L-H, Deng H-Y, Lam CH. Fragile glasses associated with a dramatic drop of entropy under supercooling. *Phys Rev Lett* 2020;125:265703.
- [49] Tanaka H. Relation between thermodynamics and kinetics of glass-forming liquids. *Phys Rev Lett* 2003;90:05570.
- [50] Richert R, Woodward WH, Fielitz T, Todd C. Using derivative plots to ascertain fragilities of glass-formers. *J Non-Cryst Solids* 2021;553:120478.
- [51] Dyre JC, Olsen NB. Landscape equivalence R. Richert Scaling vs. Vogel-Fulcher-type structural relaxation in deeply supercooled materials. *Physica A* 2000;287:26–36.
- [52] **nt of the shoving model.** *Phys Rev E* 69 (2004) 042501.
- [53] Hecksher T, Nielsen AI, Olsen NB, Dyre JC. Little evidence for dynamic divergences in ultraviscous molecular liquids. *Nat Phys* 2008;4:737–41.
- [54] McKenna GB. Diverging views on glass transition. *Nat Phys* 2008;4:673.
- [55] Martinez Garcia JC, Rzoska SJ, Drozd-Rzoska A, Martinez Garcia J. A universal description of ultraslow glass dynamics. *Nat Comm* 2013;4:1823.
- [56] Martinez Garcia JC, Rzoska SJ, Drozd-Rzoska A, Martinez Garcia J, Mauro JC. Divergent dynamics and the Kauzmann temperature in glass forming systems. *Sci Rep* 2014;4:5160.
- [57] Martinez Garcia JC, Rzoska SJ, Drozd-Rzoska A, Starzonek S, Mauro JC. Fragility and basic process energies in vitrifying system. *Sci Rep* 2015;5:8314.
- [58] Hung J-H, Patra TK, Simmons DS. Forecasting the experimental glass transition from short time relaxation data. *J Non-Cryst Solids* 2020;544:120205.
- [59] Mauro JC, Yue Y, Ellison AJ, Gupta PK, Allan DC. Viscosity of glassforming liquids. *Proc Natl Acad Sci USA* 2009;24:19780–4.
- [60] Avramov I, Milchev A. Effect of disorder on diffusion and viscosity in condensed systems. *J Non-Cryst Solids* 1988;104:253–60.
- [61] Garcia-Colin LS, del Castillo LF, Goldstein P. Theoretical basis for the Vogel-Fulcher-Tammann equation. *Phys Rev B* 1990;40:7040–444.
- [62] Richert R. Scaling vs. Vogel-Fulcher-type structural relaxation in deeply supercooled materials. *Physica A* 2000;287:26–36.
- [63] Colby RH. Dynamic scaling approach to glass formation. *Phys Rev E* 2000;61:1783–92.
- [64] Erwin BM, Colby RH. Temperature dependence of relaxation times and the length scale of cooperative motion for glass-forming liquids. *J Non-Cryst Solids* 2002;307–310:225–32.
- [65] Paluch M, Dendzik Z, Rzoska SJ. Scaling of high-pressure viscosity data in low-molecular-weight glass-forming liquids. *Phys Rev B* 1999;60:2979–82.
- [66] Elmatad YS, Chandler D, Garrahan JP. Corresponding states of structural glassformers. *J Phys Chem B* 2009;113:5563–7.
- [67] Ferreira Nascimento ML, Aparicio C. Data classification with the Vogel–Fulcher–Tammann–Hesse viscosity equation using correspondence analysis. *Phys B* 2007;398:71–7.
- [68] Mallamace F, Branca C, Corsaro C, Leone N, Spooen J, Chen S-H, et al. Transport properties of glass-forming liquids suggest that dynamic crossover temperature is as important as the glass transition temperature. *Proc Natl Acad Sci USA* 2010;107:22457–62.
- [69] Weingartner N, Pueblo C, Nogueira FS, Kelton KF, Nussinov Z. A phase space approach to supercooled liquids and a universal collapse of their viscosity. *Front Mat* 2016;3:50.
- [70] Blodgett ME, Egami T, Nussinov Z, Kelton KF. Proposal for universality in the viscosity of metallic liquids. *Sci Rep* 2015;5:13837.
- [71] Arrhenius SA. Über die Dissociationswärme und den Einfluß der Temperatur auf den Dissociationsgrad der Elektrolyte. *Z Phys Chem* 1889;4:96–116.
- [72] de Guzman J. Relación entre la Fluidéz y el Calor de Fusión. *Anales de la Sociedad Espanola de Física y Química* 1913;11:353–62.
- [73] Raman CV. A theory of the viscosity of liquids. *Nature* 1923;111:532–3.
- [74] Andrade C. A Theory of the Viscosity of Liquids. - Part I. *London Edinb Dub Philos Mag J Sci* 1934;17:497–511.
- [75] Williams G. Complex dielectric constant of dipolar compounds as a function of temperature, pressure and frequency. *Trans Faraday Soc* 1964;60:1548–55.
- [76] Williams G. Complex dielectric constant of dipolar compounds as a function of temperature, pressure and frequency. Part 2. —The  $\alpha$ -relaxation of polymethyl acrylate. *Trans Faraday Soc* 1964;60:1556–73.
- [77] Doolittle AK. Studies in Newtonian Flow. II. The Dependence of the Viscosity of Liquids on Free-Space. *J Appl Phys* 1951;22:1471–5.
- [78] Turnbull D, Cohen MH. Free-volume model of the amorphous phase: glass transition. *J Chem Phys* 1961;34:120–4.
- [79] Fox TG, Flory PJ. Second-order transition temperatures and related properties of polystyrene. *J Appl Phys* 1950;21:581–91.
- [80] Adam G, Gibbs JH. On the temperature dependence of cooperative relaxation properties in glass-forming liquids. *J Chem Phys* 1965;43:139–46.
- [81] Berthier L, Ozawa M, Scaillet C. Configurational entropy of glass-forming liquids. *J Chem Phys* 2019;150:160902.
- [82] Kauzmann W. The Nature of the Glassy State and the Behavior of Liquids at Low Temperatures. *Chem Rev* 1948;43(2):219–56.
- [83] Garrahan JP, Chandler D. Coarse-grained microscopic model of glass formers. *Proc Natl Acad Sci USA* 2003;100:9710–4.
- [84] Chandler D, Garrahan JP. Thermodynamics of coarse-grained models of supercooled liquids. *J Chem Phys* 2005;12:044511.

- [85] Wolyness PG, Bouchaud JP. **Structural Glasses and Supercooled Liquids: Theory, Experiment, and Applications**. NY: Wiley & Sons Ins; 2012.
- [86] Tanaka H, Kawasaki T, Shintani H, Watanabe K. **Critical-like behaviour of glassforming liquids**. *Nat Mater* 2010;9:324–31.
- [87] Smedskjaer MM, Mauro JC, Yue YZ. **Ionic diffusion and the topological origin of fragility in silicate glasses**. *J Chem Phys* 2009;131:244514.
- [88] Cohen MH, Grest GS. **Liquid-glass transition, a free-volume approach**. *Phys Rev B* 1982;20:1077–98.
- [89] Schmidtke B, Petzold N, Kahlau R, Hofmann V, Rössler EA. **From boiling point to glass transition temperature: Transport coefficients in molecular liquids follow three parameter scaling**. *Phys Rev E* 2012;86:041507.
- [90] Bendler JT, Shlesinger MF. Generalized Vogel law for glass-forming liquids. *J Stat Phys* 1988;53:531–41.
- [91] Bendler JT, Fontanella JJ, Shlesinger MF. A New Vogel-like law: ionic conductivity, dielectric relaxation, and viscosity near the glass transition. *Phys Rev Lett* 2001;87.
- [92] Chamberlin RV. **An Ising model for the thermal and dynamic properties of supercooled liquids and the glass transition**; 2022. <https://arxiv.org/abs/2209.05388>.
- [93] Stickel F, Fisher EW, Richert R. Dynamics of glass-forming liquids. I. Temperature-derivative analysis of dielectric relaxation data. *J Chem Phys* 1995;102:6251–7.
- [94] Corezzi S, Beiner M, Huth H, Schröter K, Capaccioli S, Casalini R, et al. **Two crossover regions in the dynamics of glass forming epoxy resins**. *J Chem Phys* 2002;117:2435–46.
- [95] Novikov VN, Sokolov AP. Universality of the dynamic crossover in glassforming liquids: a “magic” relaxation time. *Phys Rev E* 2003;67.
- [96] Roland CM. Characteristic relaxation times and their invariance to thermodynamic conditions. *Soft Matter* 2008;4:2316–22.
- [97] Götze W. **The essentials of the mode-coupling theory for glassy dynamics**. *Cond Mat Phys* 1998;1:873–904.
- [98] Götze W, Schilling R. Glass transitions and scaling laws within an alternative mode-coupling theory. *Phys Rev E* 2015;91:042117.
- [99] Drozd-Rzoska A. **A universal behavior of the apparent fragility in ultraslow glass forming systems**. *Sci Rep* 2019;9:6816.
- [100] Karmakara S, Dasgupta C, Sastry S. Growing length and time scales in glass-forming liquids. *Proc Natl Acad Sci USA* 2009;106:3575–9.
- [101] Dehaoui A, Isenmann B, Caupin F. Viscosity of deeply supercooled water and its coupling to molecular diffusion. *Proc Natl Acad Sci USA* 2015;29:12020–5.
- [102] Drozd-Rzoska A, Rzoska SJ. On the derivative-based analysis for temperature and pressure evolution of dielectric relaxation times in vitrifying liquids. *Phys Rev E* 2006;73:041502.
- [103] Dyre JC. Colloquium: The glass transition and elastic models of glass-forming liquids. *Rev Mod Phys* 2006;79:953–72.
- [104] Kremer F, Schönhal A. **Broadband Dielectric Spectroscopy**. Berlin: Springer; 2004.
- [105] Murthy SSN. Experimental study of dielectric relaxation in supercooled alcohols and polyols. *Mol Phys* 1996;87:691–709.
- [106] Popov I, Cheng S, Sokolov AP. Broadband dielectric spectroscopy and its application in polymeric materials. In: Hadjichristidis N, Gnanou Y, Matyjaszewski K, Muthukumar M, editors. *Macromolecular Engineering*. NY: Wiley; 2022.
- [107] Naoki M, Satoshi K. Contribution of hydrogen bonds to apparent mobility in supercooled D-sorbitol and some polyols. *J Phys Chem* 1991;96:431–7.
- [108] Suzuki Y. **Effect of OH groups on the polyamorphic transition of polyol aqueous solutions**. *J Chem Phys* 2019;150:224508.
- [109] Bässler H. **Viscous flow in supercooled liquids analyzed in terms of transport theory for random media with energetic disorder**. *Phys Rev Lett* 1987;58:767–70.
- [110] Drozd-Rzoska A, Rzoska SJ, Roland CM. **On the pressure evolution of dynamic properties of supercooled liquids**. *J Phys Condens Matt* 2008;20:244103.
- [111] Canorini N, Martinelli F, Roberto C. C. Toninelli **Kinetically constrained models**. In: Sidoravičius V, editor. *New Trends in Mathematical Physics*. Berlin: Springer; 2009. p. 741–52.
- [112] Keys AS, Hedges LO, Garrahan JP, Glotzer SC, Chandler D. Excitations are localized and relaxation is hierarchical in glass-forming liquids. *Phys Rev X* 2013;1:21013.
- [113] Royal CP, Turci F, Speck T. Dynamical phase transitions and their relation to structural and thermodynamic aspects of glass physics. *J Chem Phys* 2020;153:090901.
- [114] Hohenberg PC, Halperin BI. Theory of dynamic critical phenomena. *Rev Mod Phys* 1977;49:435–79.
- [115] Souletie J, Bertrand D. Glasses and spin glasses: a parallel. *J Phys (France)* 1991;11:1627–37.
- [116] Souletie J. Hierarchical scaling: An analytical approach to slow relaxations in spin glasses, glasses, and other correlated systems. *J Appl Phys* 1994;75:5512–6.
- [117] Saltzman EJ, Schweizer KS. Universal scaling, dynamic fragility, segmental relaxation, and vitrification in polymer melts. *J Chem Phys* 2004;121:2001–9.
- [118] Drozd-Rzoska A. **Heterogeneity-related dynamics in isotropic n-pentylcyano biphenyl**. *Phys Rev E* 2006;73:022501.
- [119] Drozd-Rzoska A, Rzoska SJ, Pawlus S, Martinez-Garcia JC, Tamarit J-L. Evidence for critical-like behavior in ultraslowing glass-forming systems. *Phys Rev E* 2010;82.
- [120] Martinez-Garcia JC, Martinez-Garcia J, Rzoska SJ. The new insight into dynamic crossover in glass forming liquids from the apparent enthalpy analysis. *J Chem Phys* 2012;137:064501.
- [121] Drozd-Rzoska A. **Glassy dynamics of liquid crystalline 4'-n-pentyl-4-cyanobiphenyl (5CB) in the isotropic and supercooled nematic phases**. *J Chem Phys* 2009;130:234910.
- [122] Drozd-Rzoska A. **'Quasi-Tricritical' and Glassy Dielectric Properties of a Nematic Liquid Crystalline Material**. *Crystals* 2020;10:297.
- [123] Drozd-Rzoska A, Rzoska SJ, Starzonek S. New paradigm for configurational entropy in glass-forming systems. *Sci Rep* 2022;12:3058.
- [124] Starzonek S, Drozd-Rzoska A, Rzoska SJ, Zhang K, Pawlikowska E, Kędzierska-Sar A, et al. **Gao Polivinylidene difluoride-based composite: unique glassy and pretransitional behavior**. *Europ Phys J B* 2019;93:55.
- [125] Levit R, Martinez-Garcia JC, Ochoa DA, Garcia JE. The generalized Vogel-Fulcher-Tamman equation for describing the dynamics of relaxor ferroelectrics. *Sci Rep* 2019;9:12390.
- [126] Barus C. **Isothermals, isopiestic and isometrics relative to viscosity**. *Am J Sci* 1893;45:87–96.
- [127] Rzoska SJ. New Challenges for the Pressure Evolution of the Glass Temperature. *Front Mat: Glass Sci* 2017;4:33.
- [128] Roland CM, Hensel-Bielowka S, Paluch M, Casalini R. Supercooled dynamics of glass-forming liquids and polymers under hydrostatic pressure. *Rep Prog Phys* 2005;68:1405.
- [129] Floudas G, Paluch M, Grzybowski A, Ngai K. *Molecular Dynamics of Glass-Forming Systems: Effects of Pressure*. Berlin: Springer; 2011.
- [130] Johari GP, Whalley EP. Dielectric Properties of glycerol in the range 0.1-105 Hz, 218–357 K, 0–53 kbar. *Faraday Symp Chem Soc* 1972;6:23–41.
- [131] Paluch M, Rzoska SJ, Ziolo J. On the pressure behaviour of dielectric relaxation times in supercooled, glassforming liquids. *J Phys: Condens Matt* 1998;10:4131–8.
- [132] Imre AR, Maris HJ, Williams PR. *Liquids under Negative Pressures*. Dordrecht: Kluwer; 2002.
- [133] Imre AR, Drozd-Rzoska A, Horvath A, Kraska Th, Rzoska SJ. Solid-fluid phase transitions under extreme pressures including negative ones. *J Non-Cryst Solids* 2008;354:4157–62.
- [134] Angell CA, Quing Z. **Glass in a stretched state formed by negativepressure vitrification: trapping in and relaxing out**. *Phys Re B* 1989;39:8784–7.
- [135] Kießkalt S. *Untersuchungen über den Einfluß des Druckes auf die Zähigkeit von Ölen und seine Bedeutung auf die Schmiertechnik*. Berlin: VDI-Forsch.-Heft; 1927. p. 291.
- [136] Roelands CJA. **Correlational aspects of the viscosity-temperature-pressure relationship of lubricating oils**. Doctoral dissertation Delft University of Technology, Delft; 1966.
- [137] Drozd-Rzoska A. Pressure-Related Universal Previtreous Behavior of the Structural Relaxation Time and Apparent Fragility. *Front Mat: Glass Sci* 2019;6:103.
- [138] Drozd-Rzoska A. Activation volume in superpressed glass formers. *Sci Rep* 2019;9:13787.
- [139] Bair S. Roelands' missing data. *Proc Inst Mech Engn, Part J: J Engn Tribol* 2004;218:57–60.
- [140] Bair S. High Pressure Rheology for Quantitative Elastohydrodynamics. Amsterdam: Elsevier; 2019.
- [141] Bair S, Baker M, Pallister DM. Revisiting the compressibility of oil/refrigerant lubricants. *J Tribol* 2017;139:024501.
- [142] Scarfe CM, Mysen BO, Virgo DL. **Pressure dependence of the viscosity of silicate melts**. *Geocemical Society, Special Publication No. 1*; 1987. p. 59–67.

- [143] Schubert G. **Treatise on Geophysics** (ed.). Elsevier, Amsterdam; 2015; Dingwell DB. **Properties of rocks and minerals – diffusion, viscosity, and flow of melts**. p. 473.
- [144] McEwen E. The effect of variation of viscosity with pressure on the load-carrying capacity of the oil film between gear-teeth. *J Inst Petroleum* 1952;38:646–72.
- [145] Pronin AA, Kondrin MV, Lyapin AG, Brazkhin VV, Volkov AA, Lunkenheimer P. Glassy dynamics under superhigh pressure. *Phys Rev E* 2010;81:041503.
- [146] Thoms E, Wojnarowska Z, Goodrich P, Jacquemin J, Paluch M. Inflection in the pressure dependent conductivity of the protic ionic liquid CSHIM NTF2. *J Chem Phys* 2017;146:181102.
- [147] Bair S, Martinie L, Vergne P. Classical EHL versus quantitative EHL: A perspective Part II – Super-Arrhenius piezoviscosity, an essential component of electrohydrodynamic friction missing from classical EHL. *Tribol Lett* 2016;63:38.
- [148] Sekuła M, Pawlus S, Hensel-Bielowka S, Ziolo J, Paluch M, Roland CM. Structural and secondary relaxations in supercooled di-n-butyl and diisobutyl phthalate at elevated pressures. *J Phys Chem B* 2004;108:4997–5003.
- [149] Ferreira AGM, Egas APV, Fonseca IMA, Costa AC, Abreu DC, Lobo LQ. The viscosity of glycerol. *J Chem Thermodyn* 2017;113:162–82.
- [150] Andersson SP, Andersson O. Relaxation studies of poly(propylene glycol) under high pressure. *Macromolecules* 1998;31:2999–3006.
- [151] Drozd-Rzoska A, Rzoska SJ, Paluch M. On the glass transition under extreme pressure. *J Chem Phys* 2007;126:164504.
- [152] Drozd-Rzoska A. **Pressure dependence of the glass temperature in supercooled liquids**. *Phys Rev E* 2005;72:041505.
- [153] Demus D, Pelzl G. Early case of reentrant behavior. *Liquid Crystals Today* 1995;7:531–5.
- [154] Kechin V. Thermodynamically based melting curve equation. *J Phys: Condens Matter* 1995;7:531–5.
- [155] Januchta K, Youngman RE, Goel A, Bauchy Mathieu, Logunov SL, Rzoska SJ, et al. Discovery of ultra-crack-resistant oxide glasses with adaptive networks. *ACS Chem Mat* 2017;29:5865.
- [156] Baranowski P, Starzonek S, Drozd-Rzoska A, Rzoska SJ, Bockowski M, Keblinski P, et al. Multifold pressure-induced increase of electric conductivity in LiFe<sub>0.75</sub>V<sub>0.10</sub>PO<sub>4</sub> glass. *Scientific Reports* 2019;9:16607.
- [157] Song Z, Rodríguez-Tinoco C, Mathew A, Napolitano S. Fast equilibration mechanisms in disordered materials mediated by slow liquid dynamics. *Sci Adv* 2022;8:eabm7154.